

1 *Review Paper*

2 **Accounting for Training Data Error in Machine**

3 **Learning Applied to Earth Observations**

4 **Arthur Elmes** ^{1,2*}, **Hamed Alemohammad** ³, **Ryan Avery** ⁴, **Kelly Caylor** ^{4,5}, **J. Ronald Eastman** ¹,
5 **Lewis Fishgold** ⁶, **Mark A. Friedl** ⁷, **Meha Jain** ⁸, **Divyani Kohli** ⁹, **Juan Carlos Laso Bayas** ¹⁰,
6 **Dalton Lunga** ¹¹, **Jessica L. McCarty** ¹², **Robert Gilmore Pontius Jr** ¹, **Andrew B. Reinmann** ^{13,14},
7 **John Rogan** ¹, **Lei Song** ¹, **Hristiana Stoyanova** ^{13,14}, **Su Ye** ¹, **Zhuang-Fang Yi** ¹⁵ and **Lyndon Estes** ¹

8 ¹ Graduate School of Geography, Clark University, Worcester, MA 01610, USA; reastman@clarku.edu
9 (J.R.E.); rpontius@clarku.edu (R.G.P.); jrogan@clarku.edu (J.R.); lsong@clarku.edu (L.S.); sye@clarku.edu
10 (S.Y.); lestes@clarku.edu (L.E.)

11 ² School for the Environment, University of Massachusetts Boston, Boston, MA 02125, USA;
12 arthur.elmes@umb.edu (A.E.)

13 ³ Radiant Earth Foundation, San Francisco, CA, 94105, USA; hamed@radiant.earth (H.A.)

14 ⁴ Department of Geography, University of California, Santa Barbara, CA 93013, USA; ravery@ucsb.edu (R.A.)

15 ⁵ Bren School of Environmental Science and Management, University of California, Santa Barbara, CA
16 93013, USA; caylor@ucsb.edu (K.C.)

17 ⁶ Azavea, Inc., Philadelphia, PA 19123, USA; lfishgold@azavea.com (L.F.)

18 ⁷ Department of Earth and Environment, Boston University, Boston, MA 02215; friedl@bu.edu (M.A.F.)

19 ⁸ School for Environment and Sustainability, University of Michigan, 48109, USA; mehajain@umich.edu
20 (M.J.)

21 ⁹ Faculty of Geo-Information Science & Earth Observation (ITC), University of Twente, 7514 AE Enschede,
22 The Netherlands; d.kohli@utwente.nl (D.K.)

23 ¹⁰ Center for Earth Observation and Citizen Science, Ecosystems Services and Management Program,
24 International Institute for Applied Systems Analysis (IIASA), Laxenburg, A-2361, Austria;
25 lasobaya@iiasa.ac.at (J.C.L.B.)

26 ¹¹ National Security Emerging Technologies, Oak Ridge National Laboratory, Oak Ridge, TN 37831, USA;
27 lungadd@ornl.gov (D.L.)

28 ¹² Department of Geography and Geospatial Analysis Center, Miami University, Oxford, OH 45056, USA;
29 mccartjl@MiamiOH.edu (J.L.M.)

30 ¹³ Environmental Sciences Initiative, CUNY Advanced Science Research Center, New York, NY 10065, USA;
31 areinmann@gc.cuny.edu (A.B.R.)

32 ¹⁴ Department of Geography and Environmental Science, Hunter College, New York, NY 10065, USA;
33 Hristiana.Stoyanova22@myhunter.cuny.edu (H.S.)

34 ¹⁵ Development Seed, Washington, DC 20001, USA; nana@developmentseed.org (Z.Y.)

35 *Correspondence: arthur.elmes@umb.edu, Tel. 1-304-906-7946 (A.E.); lestes@clarku.edu, Tel. 1-202-431-0496
36 (L.E.)

37 Received: date; Accepted: date; Published: date

38 **Abstract:** Remote sensing, or Earth Observation (EO), is increasingly used to understand Earth
39 system dynamics and create continuous and categorical maps of biophysical properties and land
40 cover, especially based on recent advances in machine learning (ML). ML models typically require
41 large, spatially explicit training datasets to make accurate predictions. Training data (TD) are
42 typically generated by digitizing polygons on high spatial-resolution imagery, by collecting in situ
43 data, or by using pre-existing datasets. TD are often assumed to accurately represent the truth, but
44 in practice almost always have error, stemming from (1) sample design, and (2) sample collection
45 errors. The latter is particularly relevant for image-interpreted TD, an increasingly commonly used
46 method due to its practicality and the increasing training sample size requirements of modern ML
47 algorithms. TD errors can cause substantial errors in the maps created using ML algorithms, which

48 may impact map use and interpretation. Despite these potential errors and their real-world
49 consequences for map-based decisions, TD error is often not accounted for or reported in EO
50 research. Here we review the current practices for collecting and handling TD. We identify the
51 sources of TD error, and illustrate their impacts using several case studies representing different EO
52 applications (infrastructure mapping, global surface flux estimates, and agricultural monitoring),
53 and provide guidelines for minimizing and accounting for TD errors. To harmonize terminology,
54 we distinguish TD from three other classes of data that should be used to create and assess ML
55 models: training reference data, used to assess the quality of TD during data generation; validation
56 data, used to iteratively improve models; and map reference data, used only for final accuracy
57 assessment. We focus primarily on TD, but our advice is generally applicable to all four classes, and
58 we ground our review in established best practices for map accuracy assessment literature. EO
59 researchers should start by determining the tolerable levels of map error and appropriate error
60 metrics. Next, TD error should be minimized during sample design by choosing a representative
61 spatio-temporal collection strategy, by using spatially and temporally relevant imagery and
62 ancillary data sources during TD creation, and by selecting a set of legend definitions supported by
63 the data. Furthermore, TD error can be minimized during the collection of individual samples by
64 using consensus-based collection strategies, by directly comparing interpreted training
65 observations against expert-generated training reference data to derive TD error metrics, and by
66 providing image interpreters with thorough application-specific training. We strongly advise that
67 TD error is incorporated in model outputs, either directly in bias and variance estimates or, at a
68 minimum, by documenting the sources and implications of error. TD should be fully documented
69 and made available via an open TD repository, allowing others to replicate and assess its use. To
70 guide researchers in this process, we propose three tiers of TD error accounting standards. Finally,
71 we advise researchers to clearly communicate the magnitude and impacts of TD error on map
72 outputs, with specific consideration given to the likely map audience.

73 **Keywords:** training data; machine learning; map accuracy; error propagation

74

75 1. Introduction

76 Recent technological advancements have led to a new era in Earth observation (EO, also known
77 as remote sensing), marked by rapid gains in our ability to map and measure features on the Earth's
78 surface such as land cover and land use (LCLU), e.g., [e.g. 1,2], vegetation cover and abundance [3],
79 soil moisture [4], infrastructure [5,6], vegetation phenology [7–9], land surface albedo [10–12], and
80 land surface temperature [13,14]. The resulting data are used by an expanding set of disciplines to
81 gain new insights into socioeconomic and environmental dynamics, such as community-level
82 poverty rates [15], changes in surface water [16] and forest cover [17], and carbon accounting [18]. As
83 such, EO is increasingly shaping our understanding of how the world works, and how it is changing.

84 These breakthroughs are facilitated by several technological advances, particularly the
85 increasing availability of moderate (5–30 m), high-resolution (1–5m, HR), and very high resolution
86 (<1 m, VHR) imagery, as well as new machine-learning (ML) algorithms that frequently require large,
87 high quality training datasets [19–24]. Large training datasets have been necessary for decades in the
88 production of continental and global maps [1,2,25,26]. In the current data-rich era, the impact of
89 training data (TD) quality and quantity on map accuracy is even more relevant, especially for maps
90 generated by data-hungry ML algorithms [27–32]. Errors in these products also impact the veracity
91 of any downstream products into which they are ingested [33]. While progress in algorithmic
92 performance continues apace, standards regarding the collection and use of TD remain
93 uncoordinated across researchers [34]. Additionally, much of the research and development of big
94 data and ML is occurring in industry and the fields of computer science and (non-spatial) data
95 science, leaving a potential knowledge gap for EO scientists [35,36].

96 The measurement and communication of map accuracy is a mature topic in EO and related
97 fields, with a variety of metrics and approaches tailored to different data types, analyses, and user
98 groups [37–45]. This includes substantial work to measure error in map reference data (i.e., the
99 independent sample used to assess map accuracy) and account for its impact on map assessment
100 [34,38,46,47]. However, focus on the quality and impacts of TD error has been less systematic. While
101 several efforts have been made to use and evaluate the impact of different aspects of TD quality
102 (noise, sample design, and size) on classifiers [30,32,48–53], much of this work focuses on exploring
103 these issues for specific algorithms [31,48,53,54]. Previous research shows that the impact of TD error
104 can be substantial but varied, suggesting that a more comprehensive approach to this issue is
105 warranted. Furthermore, while TD and map reference data are often collected using the same
106 approaches [55–57] and often subject to the same errors, the existing procedures to minimize and
107 account for map reference errors [34,38,46,47] are not necessarily relevant for quantifying the impacts
108 of TD error. The problems associated with TD error can be summarized as follows:

- 109 1. The “big data” era vastly increases the demand for TD.
- 110 2. ML-generated map products rely heavily on human-generated TD, which in most cases
111 contain error, particularly when developed through image interpretation.
- 112 3. Uncertainty in TD is rarely assessed or reported, and TD are often assumed to have
113 perfect accuracy [30] (which is also common with map reference data [57]).
- 114 4. TD errors may propagate to downstream products in surprising and potentially harmful
115 ways (e.g., leading to bad decisions) and can occur without the map producer and/or
116 map user’s knowledge. This problem is particularly relevant in the common case where
117 TD and reference data are collected using the same methods, and/or in cases where map
118 reference data error is not known or accounted for, which is still common [57].

119 These problems suggest a pressing need to review the issues surrounding TD quality and how
120 it impacts ML-generated maps, and to recommend a set of best practices and standards for
121 minimizing and accounting for those errors, which are the primary aims of this paper. Although map
122 error can also originate from other sources, such as the specific ML classifier selected or the
123 parameterization approach used [31,58,59], we focus solely on issues of input data quality. As such,
124 this paper complements existing work focused on assessing final map accuracy [37–41,44,45].

125 This paper is organized into four sections. In section 1, we review current practices in the
126 treatment of TD for categorical and continuous map creation. We also cover map accuracy
127 procedures, given that the two processes are often intertwined and affected by many of the same
128 issues [47], and accuracy assessment procedures are needed to assess the impacts of TD error. In
129 Section 2, we identify the most common sources of TD error and inconsistency. In section 3, we
130 illustrate the impacts of uncertainty in TD generation with case studies that span a range of typical
131 EO applications: building and road mapping, global surface flux estimates, and mapping agricultural
132 systems. In section 4, we propose guidelines for (1) best practices in collecting and using TD, (2)
133 minimizing TD errors associated with training sample design error and collection, (3) characterizing
134 and incorporating TD error in final map outputs, and (4) communicating TD error in scientific and
135 public documentation.

136 1.1. Current Trends in Training Data (TD) Collection

137 A large proportion of remote-sensing projects make some use of TD, typically created either
138 using geolocated in situ data [46,60], by visually interpreting high and/or very high spatial-resolution
139 imagery [26,61,62], or by interpreting the images to be classified/modeled themselves, e.g., [e.g.
140 55,56,63,64]. Of these collection methods, HR/VHR image interpretation is increasingly common [65],
141 particularly with the rise in crowdsourcing initiatives [22,66]. As such, mapping is strongly
142 constrained by the creation of TD, which, much like map reference data, are often treated as absolute
143 “truth”, in that their accuracy is assumed to be perfect [30,38,47,67]. However, multiple sources of
144 error are possible and indeed likely in TD, whether collected in situ or via image interpretation [60].

145 The use of large, data-intensive ML algorithms continues to grow in many fields, including
146 remote sensing. Neural networks (NN) represent an increasingly used class of ML algorithms, with
147 more complex NNs such as convolutional neural networks (CNN) producing higher output accuracy
148 [68]. While some forms of ML can function effectively with smaller training datasets, the quality of
149 these data is nevertheless critically important [28,31,51]. Additionally, the increasingly popular large-
150 scale, high-complexity NNs require substantially more TD than traditional statistical models, and
151 like many ML approaches are sensitive to noisy and biased data, producing the logistical difficulty
152 of creating very large, “clean” training datasets [69–71].

153 Partially to address this need, several recent efforts have been devoted to producing extremely
154 large training datasets that can be used across a wide range of mapping applications, and to serve as
155 comprehensive benchmarks [72,73]. Similarly, a recent trend has emerged in large-scale mapping
156 projects to employ large teams of TD interpreters, often within citizen science campaigns that rely on
157 web-based data creation tools [22,74–76].

158 1.2. Characterizing Training Data Error

159 Due to different disciplinary lineages, terminology associated with the various datasets used to
160 train and evaluate map algorithms is sometimes contradictory or disparate. Here we harmonize
161 terminology by defining four distinct types of data: training, validation, training reference, and map
162 reference. *Training data* (TD) refers to a sample of observations, typically consisting of points or
163 polygons, that relate image pixels and/or objects to semantic labels. *Validation data* are typically a
164 random subset of TD that are withheld and used to fit ML model parameters and internally evaluate
165 performance. *Training reference data* are expert-defined exemplar observations used to assess TD
166 errors during or after data creation. *Map reference data* are independent observations used to assess
167 final map accuracy; while these may be collected using many of the same procedures as the other
168 three datasets [57], they have more stringent design protocols and can only be used to assess the final
169 map product, rather than used iteratively in model or map improvement [57]. Map reference data are
170 often referred to as the test set in ML literature [77], but we use the former term to align with the
171 terminology commonly used by the EO community.

172 1.2.1. Map Accuracy Assessment Procedures

173 Map accuracy assessment practices and standards are well-established in the EO literature
174 [39,40,45,57,78]. We briefly review these procedures here because they are essential for quantifying
175 how TD error impacts map accuracy. Additionally, the growing use of ML algorithms developed
176 outside of EO has brought with it accuracy assessment practices and terminology that often differ
177 nominally or substantively from those developed for EO, e.g., [57,e.g., 79,80]. Reviewing EO accuracy
178 assessment standards can, therefore, help to harmonize and improve accuracy assessment practices,
179 while providing necessary context for procedures that can help to account for TD error.

180 The accuracy of a map is assessed by evaluating the agreement between the values of the
181 mapped variables and those of a map reference variable, and summarizing those discrepancies using
182 an accuracy metric [41,57]. The accuracy metric selected depends on whether the mapped variable is
183 categorical or continuous, since each type of variable has its own foundation for error analysis [81–
184 85]. For categorical variables, this foundation is provided by the confusion matrix, in which rows (but
185 sometimes columns) typically list how many mapped values fall within each category and columns
186 (but sometimes rows) list the distribution of map reference values for each category. In EO, the most
187 widely used metrics calculated from the confusion matrix are user’s accuracy (the complement of
188 commission error), producer’s accuracy (the complement of omission error), and overall accuracy
189 (i.e., the complement of proportion error) [40]. A fuller explanation of accuracy metrics and other
190 aspects of the error matrix can be found in existing publications [37,39,57,81,86–88]. Another widely
191 used measure in EO is the Kappa index of agreement [89], but Kappa varies with class prevalence
192 [90] and inappropriately corrects for chance agreement [57], thus its continued use is strongly
193 discouraged [40,57,91]. There are a number of other categorical accuracy metrics suitable for assessing

194 the accuracy of a binary categorical variable, such as the F1 score [80], and the true skill statistic [90],
195 which are described in the supplemental materials.

196 The scatter plot provides the basis for error analysis for continuous variables, wherein deviations
197 between the mapped values plotted on the Y-axis are measured against those of the map reference
198 on the X-axis. Several measures are used to summarize these deviations (see supplementary
199 materials). The root mean squared error (RMSE, also known as root mean square deviation, RMSD)
200 and mean absolute deviation (MAD) summarize deviations along the identity line, also referred to as
201 the 1:1 or $y = x$ line. RMSE has widespread use, but we recommend caution since it combines MAD
202 with variation among the deviations [92–94]. Another widely used measure is the R^2 , or coefficient of
203 determination, but this measures deviation relative to the linear regression line, rather than the $y = x$
204 line [82,92].

205 Beyond these, there are measures for comparing continuous mapped variables to a binary
206 reference variable, including the receiver operating characteristic (ROC) and the total operating
207 characteristic (TOC) [83,95,96]. The area under this curve (AUC) of an ROC/TOC plot is often used as
208 a single measure of overall accuracy that summarizes numerous thresholds for the continuous
209 variable [96]. There are also metrics for assessing the accuracy of object-based image analysis [OBIA,
210 97], which we do not cover here (but see the supplementary information (SI)) because the choice of
211 measure varies according to mapping objectives [65,98].

212 The creation of the map reference sample is an integral part of the accuracy assessment process
213 and has two major aspects. The first of these is the design of the sample itself (i.e., the placement of
214 sample units), which should be probability-based but can follow several different designs (e.g.,
215 simple random, stratified, cluster, systematic) depending on the application and a priori knowledge
216 of the study area [39,57]. The second aspect is the response design, which governs the procedures for
217 assigning values to the map reference samples [39,57]. These include the choice of the sample's spatial
218 and temporal units, the source of the data that the sample extracts from (e.g., high resolution
219 imagery), and the procedure for converting reference data values into map-relevant values [39,57].
220 For a categorical map in which the reference data source is high-resolution imagery, the map
221 reference sample is assigned labels corresponding to the map legend (e.g., a land-cover scheme)
222 based on a human supervisor's interpretation of the imagery [57].

223 A key aspect of response design is that map reference data should be substantially more accurate
224 than the map being assessed, even though they are always likely to have some uncertainty
225 [30,39,46,47,57]. This uncertainty should be measured and factored into the accuracy assessment
226 [39,46]. However, in practice this accounting is rarely done, while map reference data uncertainty is
227 also rarely examined [34,38,57]. This tendency is illustrated by Ye et al. [65], who reviewed 209 journal
228 articles focused on object-based image analysis, finding that one third gave incomplete information
229 about the sample design and size of their map reference data, let alone any mention of error within
230 the sample. Errors in map reference data can bias the map accuracy assessment [47,99], as well as
231 estimates derived from the confusion matrix, such as land cover class proportions and their standard
232 errors [46]. To correct for such impacts to map accuracy assessment, one can use published accuracy
233 assessment procedures, including variance estimators, that account for map reference error [38,46,47].
234 These approaches depend on quantifying errors in the map reference data.

235 1.2.2. Current Approaches for Assessing and Accounting for Training Data Error

236 Most of the aforementioned considerations regarding map reference data creation largely apply
237 to TD, particularly since map reference data and TD may often be collected together, e.g., [e.g. 55],
238 provided the former are kept strictly separate to ensure their independence [57]. Considerations
239 regarding TD may diverge with respect to sample design, as TD often need to be collected in ways
240 that deviate from probability-based sampling, in order to satisfy algorithm-specific requirements
241 related to, for example, class balance and representativeness or the size of the training sample [31,51].
242 Another difference is that map TD can be usable even with substantial error [48,50,51]—although we
243 show in Section 3 that TD error can propagate substantial map error—whereas map reference data

244 needs to have the highest possible accuracy and its uncertainty should be quantified, as described
245 above [39,46,57].

246 If the quality of map reference data is often unexamined, TD quality may be even less so. To gain
247 further insight into the level of attention TD receives in EO studies, we reviewed 30 top-ranked
248 research papers published within the previous 10 years that describe land cover mapping studies.
249 (Publications identified by Google Scholar search algorithm results; the search was performed in
250 January 2019, with terms land cover and land use mapping, including permutations of spelling and
251 punctuation. Twenty-seven articles kept after initial screening for relevance -- see Table S1
252 [2,63,64,100–123]). This assessment showed that only three papers explicitly and systematically
253 assessed the quality of the TD used in classification [2,115,122], while 16 made no mention of TD
254 standards at all. Over 75% of these studies used image interpretation, as opposed to in situ data, in
255 either training, accuracy assessment, or both. One-quarter of these papers used unsupervised
256 classifiers in the processing chain to outline training areas, followed by image interpretation to assign
257 labels to the polygons/pixels. Although only a snapshot, this finding suggests that key details
258 regarding the design and collection of TD (and even map reference data) is lacking in the EO
259 literature.

260 Even though TD quality appears to be largely unreported, efforts have been made to examine
261 how TD error can impact ML-based classifications, typically within the context of evaluating specific
262 algorithms. For example, research examining the effectiveness of random forests [124] for land-cover
263 classification also evaluated their sensitivity to TD error, sample size, and class imbalance [48,51,125];
264 similar research has been conducted for Support Vector Machines (SVM) [28,32,52]. Several studies
265 comparing multiple ML algorithms also compared how each reacted variations in TD sample size
266 and/or error [50,59,126,127]. Maxwell et al. [31] touch on a number of these TD quality issues in an
267 even broader review of ML algorithms widely used in EO classification but excluding newer deep
268 learning approaches.

269 Beyond these examples, several studies have focused more explicitly on how to train ML-
270 algorithms for remote sensing classification when TD error is present. Foody et al. [30] conducted
271 tests to examine how two different types of TD labeling error impacted land-cover classifications,
272 with a primary interest in SVM. Similarly, Mellor et al.'s [48] study measured uncertainty introduced
273 by TD error in a random forest classifier, with specific focus on class imbalance and labeling errors.
274 Swan et al. [49] examined how increasing amounts of error introduced into the TD for a deep-learning
275 model impacted its accuracy in identifying building footprints. These studies collectively
276 demonstrate that TD has substantial impact on ML-generated maps. They also reveal that there is no
277 standard, widely accepted practice for assessing TD error, which, similar to map reference data, is
278 generally not reported and thus implicitly treated as error-free [30].

279 **2. Sources and Impacts of Training Data Error**

280 In the following two sections we describe the common causes of TD error and explore its
281 potential impacts. To describe these causes, we divide the sources of TD error into two general classes:
282 (1) errors stemming from the design of the training sample, including some aspects of sample and
283 response design that are shared with standards for the collection of map reference data (see 1.2.1
284 above), and (2) errors made during the collection of the training sample, including additional
285 elements of response design such as the process of digitizing and labeling points or polygons when
286 interpreting imagery or when collecting field measurements. In addressing the impacts of error, we
287 provide a summary of potential problems, and then two concrete case examples for illustrative
288 purposes.

289 *2.1. Sources of Training Data Error*

290 *2.1.1. Design-Related Errors*

291 With respect to TD sampling design, errors primarily stem from failures to adequately represent
292 the spatial-temporal-spectral domains of the features of interest in the manner most suited to the

293 specific ML algorithm being used [53]. This problem may be exacerbated in cases where TD are
294 collected exclusively using the same rigorous probability-based specifications used to collect map
295 reference data, which may be overly restrictive for the purposes of TD collection. While the use of
296 such standards to collect TD may be possible provided that there is a large enough data set (e.g., a
297 large benchmark data set), smaller training data sets and/or cases of geographically sparse target
298 classes/objects will benefit strongly from the increased flexibility afforded to TD collection standards,
299 which are less restrictive than those for map reference data (e.g., allowing for purposive rather than
300 purely probabilistic sampling). A lack of geographic representation of the phenomena of interest
301 results in a disparity between the distribution of TD compared to the true distribution of the mapped
302 phenomenon in geographic and/or feature space [28–31]. This problem is highly relevant in ML
303 approaches, which are sensitive to TD quality, including class balance, labeling accuracy, and class
304 comprehensiveness relative to the study area’s true composition [30].

305 Temporal unrepresentativeness is also a common source of error in the response design of TD,
306 due to the prevalence of image interpretation as a source for TD. In this case, error arises when
307 obsolete imagery is interpreted to collect training points or polygons and their associated labels
308 [39,61]. The problem is illustrated in Figure 1, which contrasts smallholder fields that are clearly
309 visible in a satellite base map (Bing Maps) with ground data collected in 2018. Center pivot fields
310 were installed after the base map imagery was collected, but before ground data collection, causing
311 a temporal mismatch between the base map and the *in situ* data. Labels generated from the base map
312 would therefore introduce substantial error into an ML algorithm classifying more recent imagery.
313 New HR/VHR satellites that have more frequent acquisitions (e.g., PlanetScope [128]) can help
314 minimize such temporal gaps for projects that are designed to map present-day conditions (e.g., 2018
315 land cover), but cannot solve this problem for mapping projects covering earlier time periods (i.e.,
316 before 2016). The same can be said for aerial and unmanned aerial vehicle acquisitions, which are
317 typically limited in geographic and temporal extent [129]. While hardcopy historical maps can help
318 supplement temporal data gaps, these data sources come with their own problems, such as errors
319 introduced during scanning and co-registration, and unknown production standards and
320 undocumented mapping uncertainties.



321
322 **Figure 1.** An example of potential training data error that can arise when image interpretation is
323 conducted on older imagery. The underlying imagery is from Bing Maps, which shows smallholder
324 agricultural fields near Kulpawn, Ghana. The white polygons were collected by a team of mappers
325 (hired by Meridia) on the ground using a hand-held Global Positioning System (GPS) in 2018. The
326 smallholder fields were replaced by larger center-pivot irrigation fields sometime after the imagery
327 in the base map was collected.

328 Spatial co-registration can be a substantial source of response design error when training with
329 HR and VHR commercial satellite imagery. Due to their narrow swath widths, HR/VHR sensors are
330 often tasked, resulting in substantially off-nadir image acquisitions [61]. Due to large view zenith

331 angles and the lack of adequate digital elevation models, side overlapping imagery for stereo
332 photogrammetry, or other relevant control points, HR/VHR imagery often does not meet the same
333 orthorectification standards as coarser resolution, government-operated satellites [130–132]. When
334 integrating HR/VHR imagery acquired at different azimuth and elevation angles, features such as
335 building roofs show offsets similar to those caused by topography. These offsets are particularly
336 problematic for a) training repeated mappings of the same features, and/or b) when using an existing
337 vector dataset such as OpenStreetMap (OSM) as TD [133–135].

338 TD collected by interpreting HR/VHR imagery is often co-registered with the coarser resolution
339 imagery used as ML model data. This creates a potential spatial resolution conflict because the
340 minimum mapping unit (MMU), i.e., the relationship between image objects and pixel size, may be
341 different in the two imagery data sets. This potentially leads to situations in which objects delineated
342 as spectrally homogenous areas in HR/VHR imagery are part of mixed pixels in moderate- or coarse-
343 resolution model imagery. This mismatch is similar to the concept of H-resolution versus L-resolution
344 scene models proposed by Strahler et al. [136]; in H-resolution models, the objects of interest are
345 substantially larger than the pixel size, and vice versa for L-resolution models. The incorporation of
346 mixed pixels may degrade classification model performance, or at least introduce undesired spectral
347 variability within classes [127,137,138]. This situation may be alleviated by displaying both HR/VHR
348 imagery and/or other ancillary datasets as well as coarser model imagery during training data
349 creation [139,140]. However, such practices may not be possible when training data are taken from
350 previous research projects, or when they are to be applied in the context of time series analysis, in
351 which spatial features change over time, e.g., [e.g. 141].

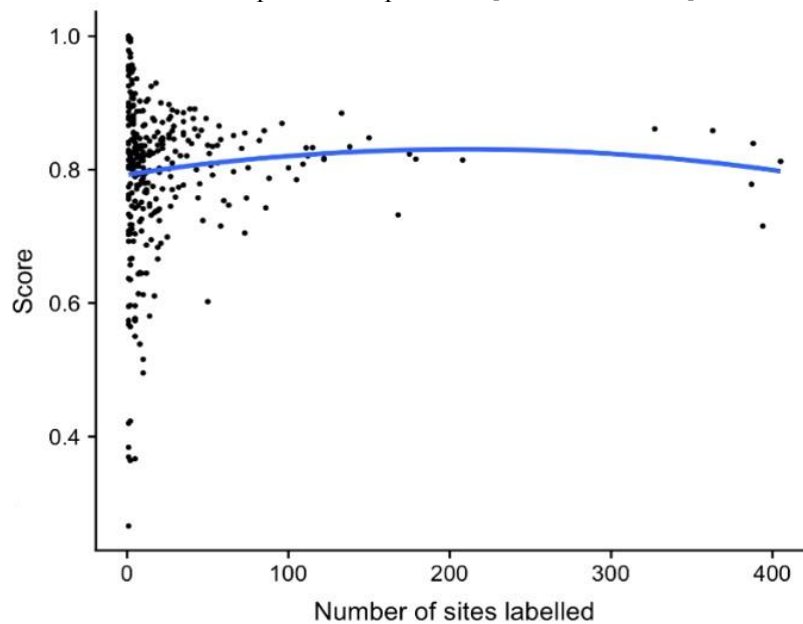
352 Similar spatial resolution and scaling issues must be dealt with when combining in situ
353 measurements with satellite observations for continuous variables. Field-collected data often cannot
354 practically cover the entire area of a pixel in the model data, especially for moderate or coarse-
355 resolution imagery, and can thus induce scaling errors related to the modifiable areal unit problem
356 [142,143]. Spatial representativeness assessments and interpolation methods are used to limit this
357 problem for operational EO science products [144–147], but this issue is likely to be a source of error
358 for most in situ TD samples.

359 Another design-related problem arises from large-scale data collection initiatives that are
360 becoming increasingly common due to the expanding extent of modern EO analyses, e.g., [e.g. 148].
361 These efforts, often conducted via crowdsourcing campaigns, typically enlist citizens to collect data
362 via a web-based platform, e.g., [66,e.g. 149–151]. Examples include OSM, Geo-Wiki [66], Collect Earth
363 [152], DIYLandcover [150], and FotoQuest Go [153]. In cases where the resulting data might be purely
364 voluntary [76], the resulting sample may lack spatial representativeness due to uneven geographic
365 contributions [28,154].

366 2.1.2. Collection-Related Errors

367 There are several common forms of error that occur when collecting both TD and map reference
368 data. The first of these are errors of interpretation [39], which are mistakes created in the process of
369 manual image interpretation. Image interpretation is widely used to generate TD, but often this
370 technique leads to inconsistent labels between interpreters for the same areas of interest
371 [34,37,99,155]. Interpreters may lack experience in the task or be unfamiliar with the context of the
372 study area, e.g., [e.g. 156]. In an unusually thorough analysis of error in image interpretation, Powell
373 et al. [99] showed that inter-interpreter agreement was on average 86% but ranged from 46 to 92%,
374 depending on land cover. This research, which relied on trained image interpreters, concluded that
375 transitional land cover classes produce substantial interpretation uncertainty, which is particularly
376 problematic since much land cover mapping effort is directed towards change detection. Another
377 image interpretation study that used a crowdsourcing platform found that interpreters' average
378 accuracy in digitizing crop field boundaries in high-resolution imagery was ~80%, based on
379 comparisons against training reference data [150]. This result held true whether the interpreters
380 mapped several hundred sites or <50 (Figure 2), indicating that increased interpreter experience does
381 not necessarily eliminate labeling error, even when analysts are highly seasoned [99]. These findings

382 underscore the need to assess uncertainty in TD, as well as map reference data, using predefined
 383 training reference data or inter-interpreter comparisons [46,60,99,157,158].



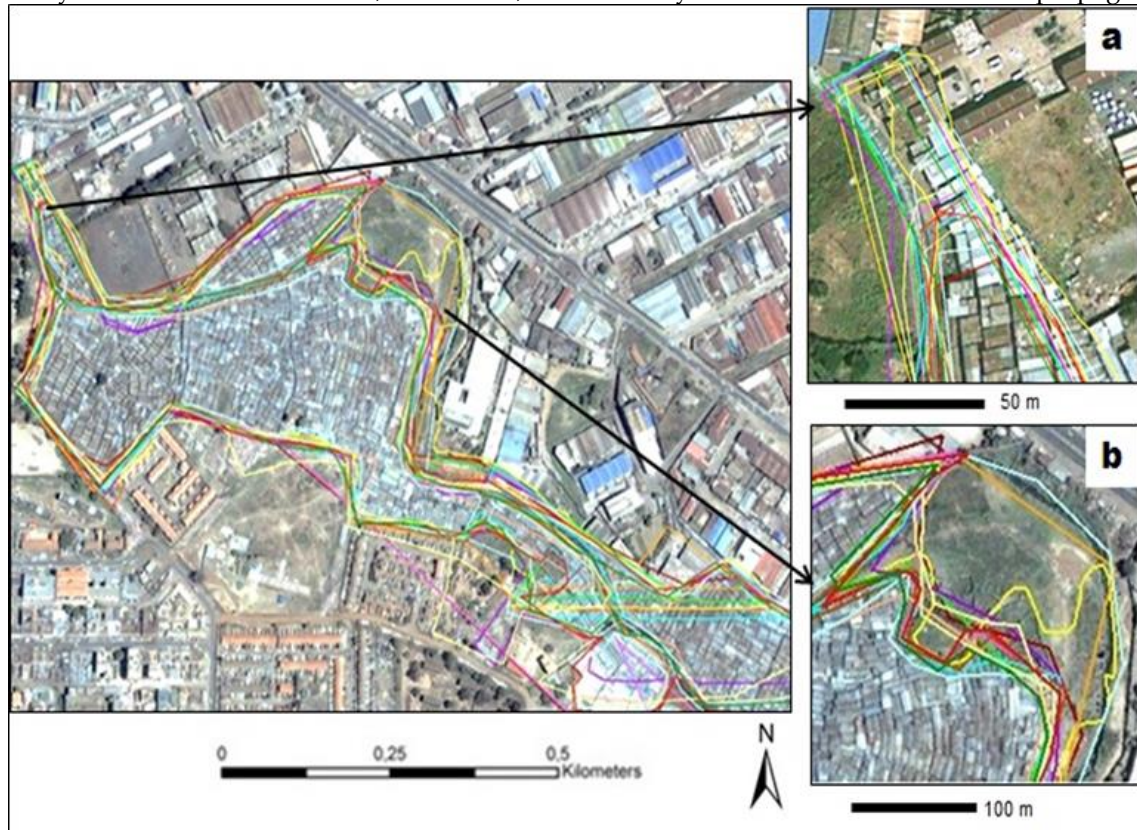
384

385 **Figure 2.** Number of sites mapped per worker versus the average score received at reference sites,
 386 where workers' maps were compared to reference maps using a built-in accuracy assessment protocol
 387 within a crowdsourcing platform for collect cropland data [150].

388 Labeling error may also result from inadequate or poorly communicated semantic class
 389 definitions [159,160], particularly when identifying human land use as opposed to biophysical land
 390 cover [161]. This is especially evident in urban environments, which exhibit high spatial and spectral
 391 heterogeneity (even within HR/VHR imagery [162]), and are also semantically vague (i.e., hard to
 392 define) even at the ground level. For example, Figure 3 shows a typical example of TD collection for
 393 mapping informal settlements (i.e., slums), in Nairobi, Kenya, in which several trained interpreters
 394 separately delineate the same area [163]. Because slums may be defined by sociodemographic factors
 395 in addition to spatial and spectral properties, TD creation for such areas is prone to error stemming
 396 from semantic issues [160]. Complex classes such as slums may exhibit high variability between study
 397 areas, as local idiosyncrasies link the definition of slums to different physical, remotely observable
 398 characteristics. These characteristics make it hard to develop a generalizable mapping capability for
 399 land uses such as informal settlements. These results further illustrate the importance of consensus
 400 mapping for image interpretation, particularly for spatially, spectrally, or temporally heterogeneous
 401 LCLU classes, which may have vague or regionally idiosyncratic semantic definitions.

402 Categorical mapping projects typically define a crisp set of non-overlapping categories, rather
 403 than a fuzzy set [164,165]. However, many human and natural land covers exhibit continuous
 404 gradation between classes, implying that crisp map legends will necessarily cause semantic
 405 ambiguity when image pixels in transitional areas are labeled [166,167]. This problem is particularly
 406 acute with moderate- and coarse-resolution imagery [26]. Local variance is highest when scene
 407 objects approximate the spatial dimension of the image resolution, leading to poor classification
 408 accuracy [168]. While substantial research has been devoted to the issue of mixed pixels
 409 [85,137,138,169–171], crisp categories are still often relied on during the training and testing phases
 410 of image classification [172]. Alternative approaches based on fuzzy set theory are available, but have
 411 seen limited adoption [165,173]. Labeling errors can also arise if analysts are not properly trained
 412 regarding class definitions, or by the failure to capture comprehensive metadata while collecting TD
 413 in the field or during image interpretation. Lack of TD metadata is particularly problematic in the
 414 context of difficult-to-determine labeling cases, or when there is potential confusion between
 415 spectrally, spatially, or semantically/conceptually similar classes [161]. Such inadequacies limit the

416 analysis of TD error and, therefore, the ability to account for error propagation.



417

418 **Figure 3.** The challenges of mapping slum extent from image interpretation in Nairobi, Kenya. Each
 419 colored line indicates a different analyst's delineation of the same slum, illustrating semantic
 420 confusion. Adapted with permission from Kohli et al. [163].

421 Collection-related errors may be particularly acute in large-scale crowdsourcing campaigns or
 422 citizen science initiatives, which are increasingly valued for mapping projects due to their larger size
 423 and cheaper acquisition costs [22,66,150,151]. Such datasets are often collected rapidly and entail
 424 labeling many observations over a short period of time by participants who are not domain experts
 425 [153,174]. In such cases, label quality is a function of interpreter skill, experience, contextual
 426 knowledge, personal interest, and motivation for involvement in the data collection [22]. Errors can
 427 be exacerbated if interpreters are inadequately trained or unfamiliar with the study area, or lack
 428 experience with EO data and methods. For example, delineation of different classes of urban land use
 429 may be extremely difficult without the benefit of local knowledge [160]. Furthermore, image
 430 interpretation is complicated when participants are required to interpret HR/VHR satellite imagery
 431 collected over multiple sensors, on different acquisition dates, with varying quality (e.g., cloud cover
 432 percentage and atmospheric correction), and/or with varying view/sun angles [175]. Inadequate or
 433 confusing user interfaces may also lead to error [22,160]. Once crowdsourced/citizen science data
 434 have been post-processed for noise, they can be highly detailed and spatially extensive [66,69–71].
 435 Nevertheless, quality problems in such datasets can be particularly hard to find and clean and are
 436 thus an important source of TD error that may propagate through ML algorithms into map outputs
 437 [57,151,176]. Therefore, these data should be used more cautiously than expert-derived TD.

438 Errors also arise in in situ TD, caused by measurement error, geolocation inaccuracy, or incorrect
 439 identification of relevant objects (e.g., vegetation species), for example [177]. In addition to these
 440 factors, some feature types may also be difficult to discern on the ground [30]. Aside from these
 441 problems, there are many sources of technologically induced errors, such as defects in the software
 442 or hardware of measurement devices, user input error, or calibration errors (e.g., in spectro-
 443 radiometers or other equipment). However, accounting for quantitative measurement error is more
 444 straightforward than thematic TD creation. Textbook tools to quantify measurement error are widely

445 available, and in situ data collection procedures often include inter-analyst measurement
446 comparison [178,179].

447 2.2. Impacts of Training Data Error

448 TD errors carry through to impact the map production process and outcomes. From a design
449 perspective, the size and class composition of TD is particularly impactful on ML algorithms, which
450 are susceptible to overfitting and class imbalance problems [31,73]. Additionally, the assumption of
451 representativeness of training pixels is often overstated, and many TD may in fact not be
452 generalizable to broader scales (discussed by Tuia et al. [154]). TD errors arising from the collection
453 process also impact map quality. Both design- and collection-related errors may be particularly hard
454 to discern, or quantify in absolute terms, if the error in the map reference data errors are unknown.

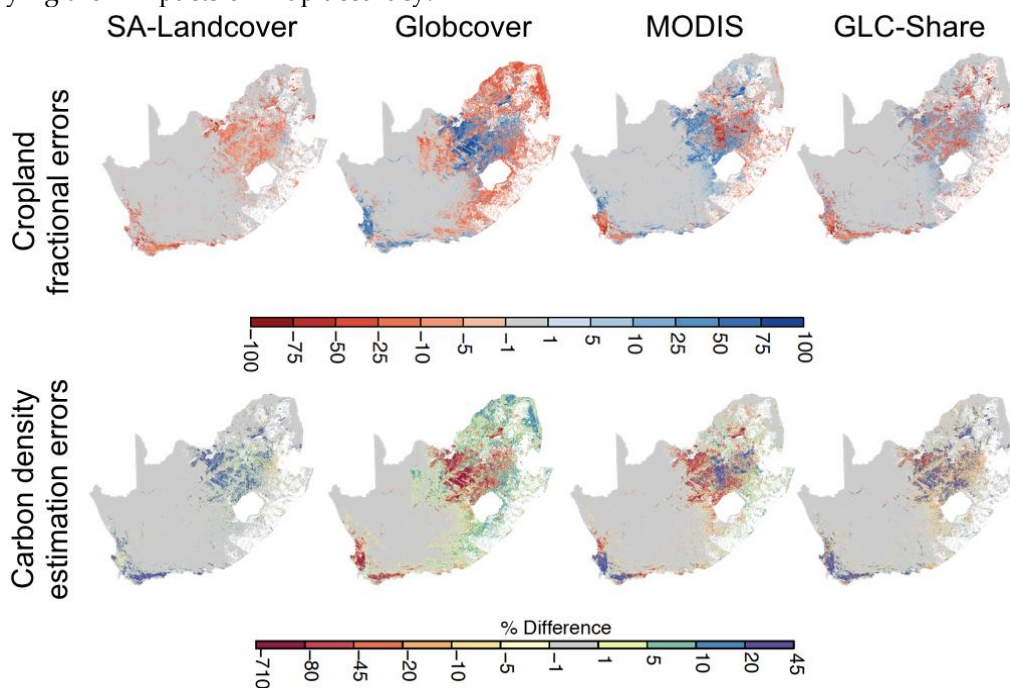
455 Several studies reviewed in Section 1.2.2 provide insight into how much TD error can impact
456 ML-generated land-cover maps, focusing on aspects of sample size and balance (design-related
457 errors) and labeling error (collection-related error). This work shows that the impact of each error
458 source varies according to the algorithm used. For example, SVMs were relatively insensitive to
459 changes in sample size, with accuracy dropping by only 3%–6% under TD size reductions of 85%–
460 94% [28,180]. Random forests (RF) also proved robust to TD sample size, showing slightly higher
461 accuracy drops of ~4%–10% when TD was reduced by 70%–99% [48,51,180]. Sample size also
462 impacts the certainty of RF classification by lowering the mean margin (a measure of certainty related
463 to the number of class votes) by ~50% for sample size reductions of 95% [48]. In contrast to SVM and
464 RF, maps classified with single decision trees are highly affected by TD size, with 13% accuracy loss
465 for TD reductions of 85% [28], and up to 50%–85% loss with TD size reductions of 50%–70% [51,59].
466 NNs show varying responses to sample size, depending on their algorithmic design: one NN based
467 on adaptive resonance theory showed accuracy reductions of ~30% to ~65% when TD samples were
468 halved [59], while a feed-forward NN lost just 2% accuracy when TD was reduced by 85% [28].

469 Classifiers are also sensitive to class balance within the training data. For example, the accuracy
470 of RF-generated maps declined by ~12% to ~23% and classification confidence fell ~25% to ~50% when
471 TD class balances were highly skewed [48]. Notably, the ranges in these accuracy and confidence
472 declines were attributable to differing TD sample sizes, showing the synergistic effect of sample size
473 and class balance sensitivities. Maxwell et al. [31] provide a more comprehensive review of class
474 imbalance for RF, SVM, NN, and k-nearest neighbors (kNN) classifiers, finding that all models were
475 sensitive to class imbalance, but the accuracy impact was largest for rare classes, as opposed to overall
476 map accuracy.

477 The impact of TD labeling errors, also referred to as noise, varies substantially between mapping
478 algorithms. SVMs and closely related derivatives appear least sensitive to mislabeling. SVMs lost just
479 0%–5% in land-cover classification accuracy when 20%–30% of TD samples were mislabeled either
480 randomly or uniformly across classes [30,52,126]. Relative vector machines (RVMs) were even less
481 sensitive under these conditions (2.5% accuracy loss for 20% mislabeling [30]), and an SVM designed
482 specifically for handling noisy TD (context-sensitive semi-supervised SVM) was even more robust
483 (2.4% reduction in kappa for 28% mislabeling [52]). However, the impact of TD noise was greater for
484 all three models when mislabeling was confined to specific classes. SVMs lost 9% accuracy and 31%
485 kappa when 20%–28% of samples in spectrally similar classes were mislabeled [30,52]. The RVM
486 showed a 6% accuracy loss [30], and the specialized SVM showed a 12% kappa reduction [52] under
487 the same conditions. As with sample size, RF is the next least sensitive to TD noise [48,51]. Mislabeling
488 25% of TD samples reduced RF accuracy by 3%–7% for a binary classifier and 7%–10% for a multiclass
489 model, with the ranges in accuracy loss also varying according to TD sample size [48]. Classification
490 certainty was more heavily impacted by label error, dropping by 45%–55%, as measured by the mean
491 margin [48]. Other classification models showed larger impacts due to label noise, including 11%–
492 41% kappa declines for a kNN (28% label noise [52]), and 24% [126,181] and 40%–43% accuracy loss
493 for a kernel perceptron and NN, respectively, when each is trained with 30% of TD labeled incorrectly
494 [59,126,181]. Single decision-tree models were most sensitive to label error, registering 39% to nearly
495 70% accuracy declines for 30% label noise [59,126,181].

496 The research described above provides substantial information on how TD error can impact the
 497 accuracy and certainty of older-generation ML classifiers. Further understanding of the consequences
 498 of these errors can be inferred from literature examining the impact of errors in map reference data.
 499 Map reference errors can substantially bias areal estimates of land-cover classes, as well as the
 500 estimation of variance in those classes, particularly when examining land-cover change [46,182,183].
 501 While methods exist to incorporate map reference data error into map accuracy assessments and area
 502 estimates [38,46,47], and also to account for TD uncertainty in assessing classifier accuracy [48], there
 503 has been little work that shows how to address both TD and map reference error.

504 Less information is available regarding the ways in which TD error may propagate beyond the
 505 map it initially creates. Initial research by Estes et al. [33] examined how error propagates from a
 506 primary land-cover map into subsequent derived products. This work used a high-quality reference
 507 cropland map to quantify the errors in 1 km cropland fractions derived from existing land cover
 508 datasets and measured how these errors propagated in several map-based analyses drawing on
 509 cropland fractions for inputs. The results suggest that downstream errors were in some instances
 510 several fold larger than those in the input cropland maps (e.g., carbon stock estimates, Figure 4),
 511 whereas in other cases (e.g., evapotranspiration estimates) errors were muted. In either case, the
 512 degree to which the error magnifies or reduces in subsequent maps is difficult to anticipate, and the
 513 high likelihood that error could increase means that any conclusions based on such land cover-
 514 derived maps must be treated with caution when error propagation is not quantified. This analysis
 515 suggests how TD errors might impact the maps they generate and provides a potential method for
 516 quantifying their impacts on map accuracy.

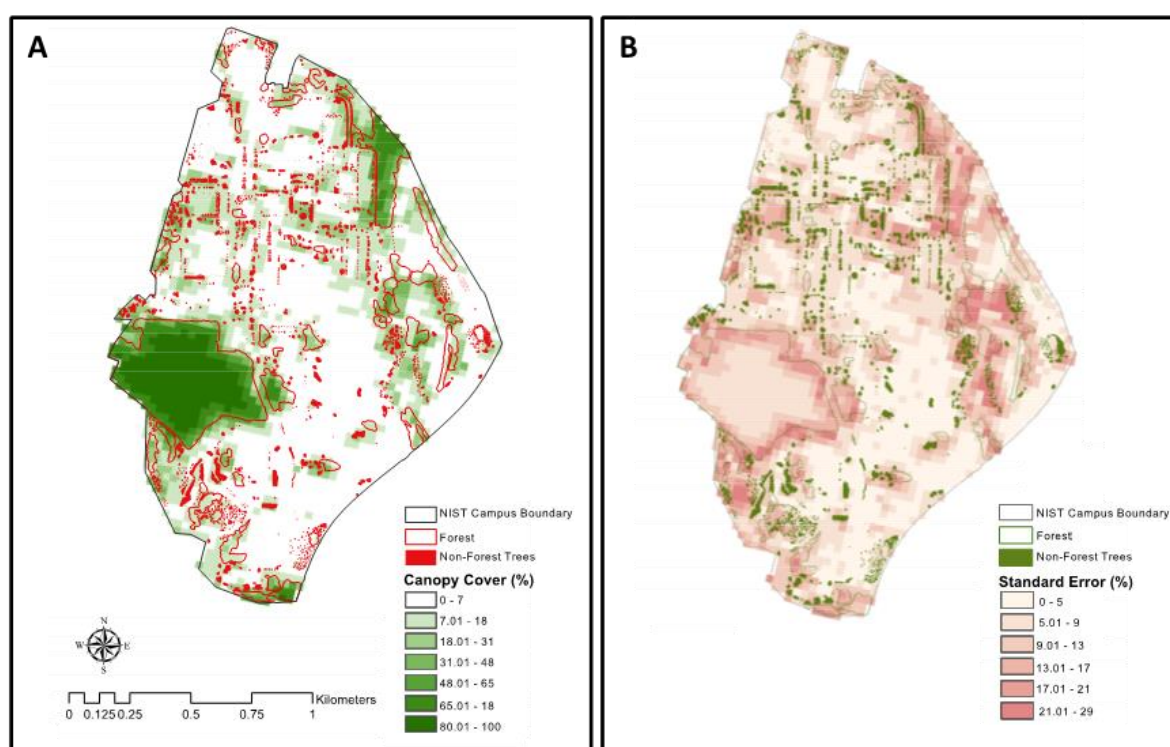


517

518 **Figure 4.** An examination of how error in pixel-wise cropland fractional estimates (expressed as a
 519 percentage, top row) can propagate error (expressed as a percentage) in maps that use land-cover
 520 data as inputs, such as estimates of carbon density (bottom row). Figure adapted from Estes et al. [33].

521 The impact of map input errors can also be seen in the practice of using well-known standard
 522 datasets, such as the National Land Cover Map [NLCD, 184], to map quantities of interest, such as
 523 urban tree canopy biomass. Urban trees play a crucial role but in regional carbon cycles [185–187] but
 524 are often omitted from EO studies of carbon dynamics, e.g., MODIS Net Primary Productivity [e.g.,
 525 MODIS NPP, 188]. As urban lands are expected to triple between 2000 and 2030 [189,190], the need
 526 to factor them into carbon accounting is pressing, but remotely mapping urban tree cover is limited
 527 by (a) spatial resolutions that are too coarse for highly variable urban landscapes and (b) TD that are
 528 often biased to forested, agricultural, and other rural landscapes. For these reasons, the Landsat-

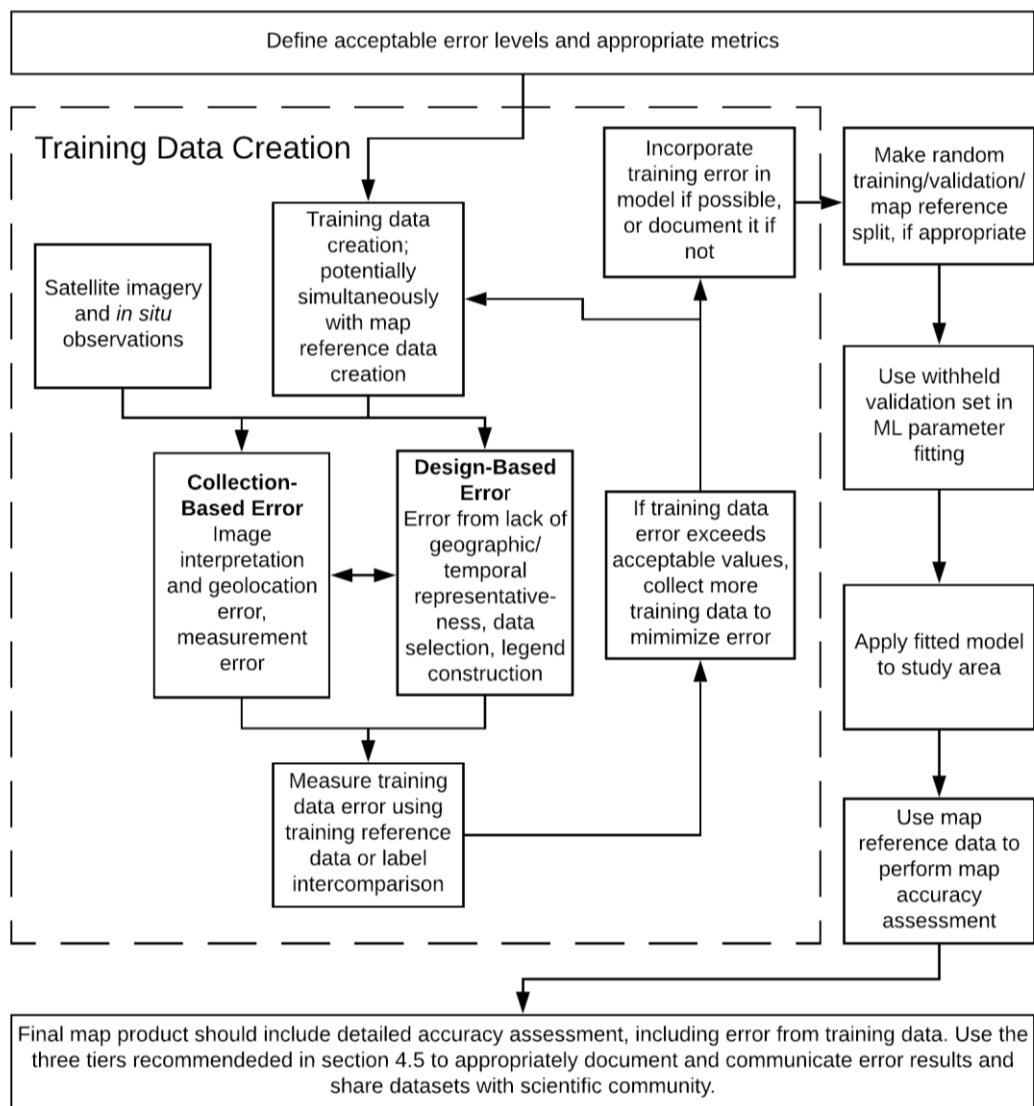
529 derived NLCD Percent Tree Cover (PTC) product [191], which estimates canopy cover at 30-m
 530 resolution across the US, provides a practical input for empirical models to map tree biomass.
 531 However, previous studies have shown that this product shows higher uncertainty in urban areas
 532 [191] and has a tendency to underestimate urban canopy cover compared to high resolution datasets.
 533 Therefore, to quantify the potential impact of NLCD PTC error on canopy biomass estimates, we
 534 compared the accuracy of the NLCD PTC dataset to canopy cover estimates derived from manually
 535 digitized VHR Imagery for a suburb of Washington, D.C., USA. We found that NLCD PTC
 536 underestimated canopy cover by 15.9%, particularly along forest edges (Figure 5) where it
 537 underestimated canopy cover by 27%. This discrepancy is particularly important in heterogeneous
 538 urban landscapes, where forest edges comprise a high proportion of total forest area. Scaling field
 539 data from forest plots to the entire study yielded an estimate of 8164 Mg C stored in aboveground
 540 forest biomass, based on our manually digitized canopy cover map, compared to only 5960 Mg C
 541 based on the NLCD PTC. This finding indicates the significance of these map errors for carbon
 542 accounting, as temperate forest carbon storage and rates of sequestration are much larger (64% and
 543 89%, respectively) than in forest interiors [192]. Quantifying errors in the NLCD is thus important for
 544 correcting subsequent estimates trained on these data.
 545



546 **Figure 5.** Spatial variations in canopy cover (A) and uncertainty in canopy cover estimates (B) in
 547 forested and non-forested areas of the heterogeneous suburban landscape of the National Institute of
 548 Standards and Technology campus in Gaithersburg, Maryland. Percent canopy cover at a 30-m
 549 resolution from the commonly used National Land Cover Database (NLCD) Percent Canopy Cover
 550 product (and its uncertainty) is superimposed over a high-resolution map of forested areas (hollow
 551 outlined polygons) and non-forest trees (e.g., street trees; solid polygons) that were manually mapped
 552 using <1-m resolution Wayback World Imagery. Note the lower estimates of percent canopy cover
 553 along forest edges (A) and the associated higher levels of uncertainty (B) using the NLCD product.

554 These brief examples help illustrate the potential problems of TD error, but the range of potential
 555 impacts is as varied as the number of mapping projects underway across academic research,
 556 commercial operations, and the public sphere. To represent the growing set of remote-sensing
 557 applications in which TD error may be encountered, we present a set of case studies below. To help
 558 lay a common framework, we show a typical methods sequence for a ML-based remote-sensing
 559 analysis in Figure 6, which also helps clarify the terminology used in this paper. The figure shows

560 the various sources and implications of error in the modeling and mapping process, beginning with
 561 issues in the data sources and sample design, and continuing through-model training, validation,
 562 and ultimately in map accuracy assessment.



563

564

565

Figure 6. Flow chart of typical workflow for machine-learning applications in Earth observation data.

566

3. Case Studies

567

568

569

To better illustrate the potential impact of TD error, we provide several case studies across different mapping applications that represent the broad range of ML-based mapping and modeling applications that rely on TD.

570

3.1. Infrastructure Mapping

571

3.1.1. Incorporating Noisy Training Label Data

572

573

574

575

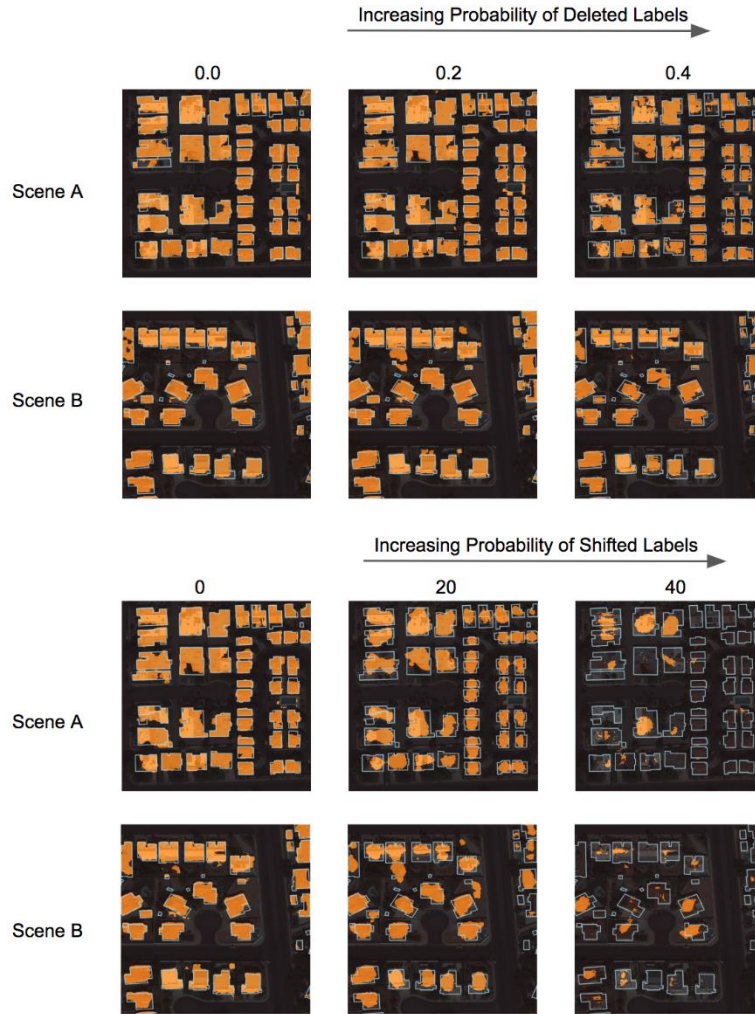
576

Automated building footprint detection is an important but difficult mapping task, with potential benefits for a wide range of applications. The following case study illustrates the use of Raster Vision (<https://rastervision.io/>), an open source deep learning framework, to train several models for automated building detection from high resolution imagery (Additional detail available at: <https://www.azavea.com/blog/2019/08/05/noisy-labels-deep-learning/>). These models perform

577 best when trained on a large number of correctly labeled examples, usually generated by a paid team
578 of expert labelers. An alternative, less costly approach was conducted in which a building
579 segmentation model was trained using labels extracted from OSM. However, the labeled training
580 polygons generated from OSM contain errors: some buildings are missing, and others are poorly
581 aligned with the imagery or have missing details. This provides a good test case for experimentation
582 on how noise in the labels affects the accuracy of the resulting model.

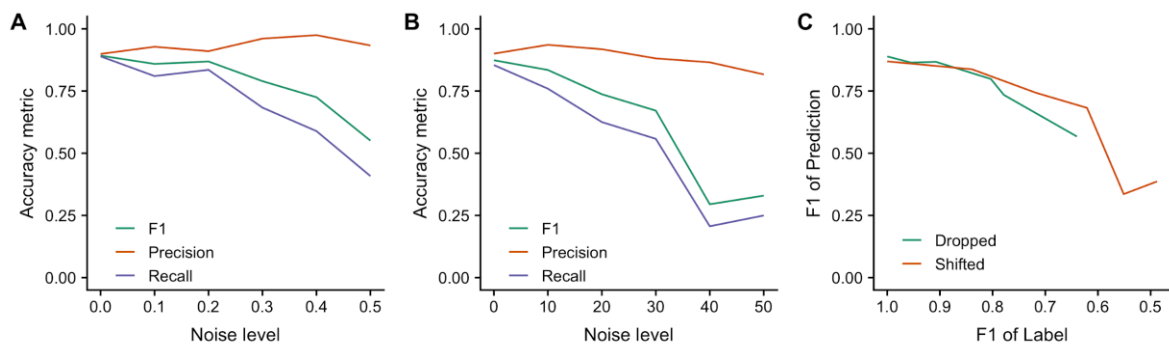
583 To measure the relationship between label noise and model accuracy, the amount of label noise
584 was varied while holding all other variables constant. To do this, an off-the-shelf dataset (the
585 SpaceNet Vegas buildings data set) was used in place of OSM, into which label errors were
586 systematically introduced. Missing and imprecisely drawn building errors were systematically
587 introduced to this relatively large training data set (~30,000 labeled buildings)
588 (<https://spacenetchallenge.github.io/datasets/spacenetBuildings-V2summary.html>), and then the
589 resulting model accuracy was measured. The experimental design consisted of two series of six
590 datasets each, with random deletion or shift of buildings at increasing probabilities and magnitudes,
591 respectively. For each dataset, a UNet semantic segmentation model with a ResNet18 backbone was
592 trained using the fastai/PyTorch plugin for Raster Vision ([https://github.com/azavea/raster-vision-](https://github.com/azavea/raster-vision-fastai-plugin)
593 [fastai-plugin](https://github.com/azavea/raster-vision-fastai-plugin)). These experiments, including data preparation and visualization, can be replicated
594 using `code` at [https://github.com/azavea/raster-vision-](https://github.com/azavea/raster-vision-experiments/tree/master/noisy_buildings_semseg)
595 [experiments/tree/master/noisy_buildings_semseg](https://github.com/azavea/raster-vision-experiments/tree/master/noisy_buildings_semseg).

596 Figure 7 shows the ground truth and predictions for a variety of scenes and noise levels, showing
597 that the quality of the predictions decreases with the noise level. The background and central portions
598 of buildings tend to be predicted correctly, whereas the outer periphery of buildings presented a
599 greater challenge. These results are quantified in Figure 8, which shows F1, precision, and recall
600 values for each of the noise levels below (see Table S2 for terminology description). The precision
601 falls more slowly than recall (and even increases for noisy drops), which is consistent with the pattern
602 of errors observed in the prediction plots. Pixels that are predicted as building tend to be in the central
603 portion of buildings, leading to high precision.



604
605
606
607

Figure 7. Predictions of the model trained on different noisy datasets. Each row shows a single scene over different noise levels. The top two rows show noisy drops, while the bottom two rows show noisy shifts. The ground truth is outlined in light blue, and the predictions are filled in orange.



608
609
610
611
612

Figure 8. The precision, recall, and F1 scores across different noise levels are shown for the cases in which labels are randomly dropped (A) or randomly shifted (B). Panel (C) compares how prediction quality changes as noise increases for dropped and shifted labels, measured by F1 of the labels and prediction.

613
614
615
616

In panels (A) and (B) of Figure 8, the x-axis shows the noise from randomly dropped and randomly shifted labels, respectively. Panel (C) combines the effects of noisy deletions and noisy shifts on accuracy in a single graph, showing F1 of the labels on the x-axis and F1 of the prediction on the y-axis. The F1 score of the noisy versus ground truth labels is a function of the pixel-wise

617 errors; this metric has the benefit of measuring the effect of noise on error in a way that is comparable
618 across datasets and object classes. For instance, a noisy shift of 10 in a dataset with large buildings
619 might result in a different proportion of erroneous label pixels than in another dataset with small
620 buildings. From this, panel (C) shows that while some of the shifted datasets have a greater level of
621 noise, the prediction F1 scores are similar between the two series when the noise level is similar.

622 These results present a small step toward determining how much accuracy is sacrificed by using
623 TD from OSM. Preliminary results indicate that accuracy decreases as noise increases, and that the
624 model becomes more conservative as the noise level increases, only predicting central portions of
625 buildings. Furthermore, the noisy shift experiments suggest that the relationship between noise level
626 and accuracy is non-linear. Future work will quantify the functional form of this relationship, and
627 how it varies with the size of the training set. Some preliminary work toward this goal has been
628 described in Rolnick et al. [193], which focuses on image classification of Imagenet-style images.

629 One limitation of these results is that the magnitude of error in OSM for most areas is unknown,
630 making it difficult to predict the effect of using OSM labels to train models in a generalized, global
631 sense. Noisy error in OSM can be estimated by measuring the disparity between OSM labels to clean
632 labels, such as the SpaceNet labels used here, providing a local estimate of OSM noise. A more general
633 but less rigorous approach is to roughly estimate the noise level by visually inspecting the labels in
634 OSM, and comparing to Figure 7, which shows examples of the labels at different noise levels.

635 3.1.2. Detecting Roads from Satellite Imagery

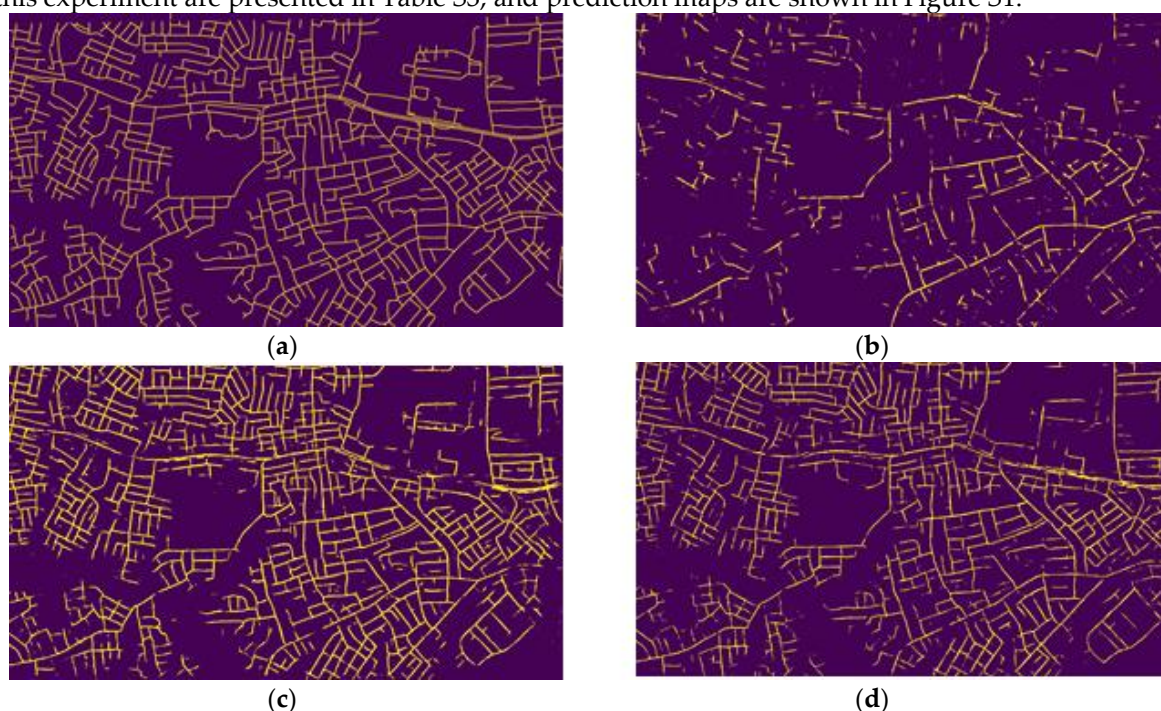
636 Road networks constitute a critical geographical data layer used to assist national decision
637 makers in resource allocation, infrastructure planning, vaccination campaigns, and disaster response,
638 among others. However, accurate and up-to-date road networks are not available in many
639 developing countries. High-resolution satellite imagery, paired with deep-learning methods,
640 provides the capacity to detect and map roads at large spatial scales. This important goal, however,
641 is dependent on availability of local high-quality TD.

642 To evaluate the impact of local TD availability on predicted road network accuracy, a study was
643 carried out in Kumasi, Ghana [194]. Two datasets were used to train ML models: (1) the SpaceNet
644 (<https://spacenetchallenge.github.io/>) dataset [195] in Khartoum, Sudan, and Las Vegas, USA, and (2)
645 OSM data in Kumasi, Ghana. The SpaceNet Dataset includes high quality road labels with human
646 expert validation, but unfortunately was not available in Kumasi, Ghana. Therefore, the latter study
647 site relied on OSM data, consisting of crowdsourced labels with no accuracy assessment or expert
648 validation. A series of experiments were carried out to assess the feasibility of using transfer learning,
649 using the Raster Vision Python library for training and evaluation. For all MobileNet V2 models
650 introduced in the following list, the image chip size was set to 300×300 pixels, and the
651 training/validation split was 80/20.

652 The Las Vegas Model was trained and validated on SpaceNet data in Las Vegas and produced
653 very high accuracy predictions. However, when this model was used in Kumasi, it predicted very
654 few roads, with only scattered road segments. The Khartoum model was also trained using SpaceNet
655 data in Khartoum. The Kumasi model used Maxar WorldView-3 imagery and labels from OSM as
656 input. OSM was used to test the quality of crowdsourced labels in training a road detection model.
657 The Khartoum Model was then fine-tuned on OSM labels in Kumasi for three different steps of 100
658 K, 50 K and 10 K. All models used the same hyperparameters, to isolate the role of TD on model
659 performances.

660 To validate the models' performance using an independent dataset, a set of expert labels was
661 generated over a small part of Kumasi. Figure 9 shows the region with human expert data vetting,
662 along with the three model predictions. The Las Vegas model is excluded from this figure as it does
663 not have any meaningful prediction in Kumasi. Quantitative performance metrics were calculated
664 using the expert-created labels, to which the models had been blind during training. The results
665 indicate that, as shown by Figure 9, the F1 score for roads was substantially higher for the Kumasi
666 model (0.6458) than when using the Khartoum model (0.3780). However, by retraining and fine-

667 tuning the Khartoum model, the F1 score for roads increased to 0.6135. The full accuracy results for
 668 this experiment are presented in Table S3, and prediction maps are shown in Figure S1.



669 **Figure 9.** (a) Labels generated by experts for validation. (b) Predictions from the Khartoum model. (c)
 670 Predictions from Kumasi model. (d) Predictions from Khartoum model retrained in Kumasi with 10
 671 K steps.

672 Based on these results, it is concluded that: (1) lack of diverse TD significantly limits the
 673 geographic applicability of models, as the types, surfaces, and arrangements of roads varies
 674 substantially between regions; (2) regional training datasets are essential for the model to learn the
 675 feature of roads in that region; and (3) transfer learning from a reasonably similar geography can help
 676 train models.

677 3.2. Global Surface Flux Estimates

678 Fluxes at the land–atmosphere boundary play a key role in regulating water, carbon and energy
 679 cycles. These fluxes include latent heat flux (LE), sensible heat flux (H), and gross primary production
 680 (GPP). While these fluxes cannot be measured directly from remote-sensing observations, other
 681 remotely sensed variables can be used to estimate these fluxes. Moreover, these three fluxes are
 682 highly coupled and, therefore, a coupled model is ideal.

683 A fully connected neural network model was developed for this purpose [196], named water,
 684 energy, and carbon with artificial neural networks (WECANN). Inputs to WECANN are remotely
 685 sensed estimates of precipitation, soil moisture, net radiation, snow water equivalent, air temperature
 686 and solar induced fluorescence. The target variables for training the model were derived from
 687 outputs of global models. However, this presents the difficulty that the target variables are model
 688 outputs that can have substantial error, which will propagate in the WECANN model. To mitigate
 689 this problem, three independent estimates of each of the three fluxes (LE, H and GPP) were retrieved
 690 from the global models. Then a novel statistical approach, named triple collocation (TC, Figure S2,
 691 equation S1), was used to combine those estimates to a new dataset for training the WECANN model.

692 Triple collocation (TC) is a technique for estimating the unknown error (measured with standard
 693 deviations or RMSEs) of three mutually independent measurement systems, without treating any
 694 one system as zero-error “truth” [197]. The three measurement systems estimate a variable collocated
 695 in space and time, hence the name triple collocation. Using these probabilities, at each pixel and at
 696 each time one of the three estimates of the target variable is randomly selected to generate the TD.

697 The results of WECANN model outputs were evaluated against ground measurements from
698 global FLUXNET towers from 2007 to 2015 (Figure 10), using both the coefficient of determination
699 and RMSE to evaluate accuracy. These show that WECANN's correlation was on average 17% higher
700 (range 8%–51%) than that of any one of the three individual inputs, while the RMSE was 21% lower
701 (range 4%–54%). These differences provide a partial quantification of the error inherent in any one of
702 these training inputs and show that by combining them using the TC technique, we can reduce error
703 in an ML model for predicting the fluxes at global scale. This case study illustrates a means of
704 assessing and accounting for error in TD for cases in which these data are not created specifically for
705 the project, but rather are pre-existing data products with potentially quite different characteristics
706 and potentially unknown error.

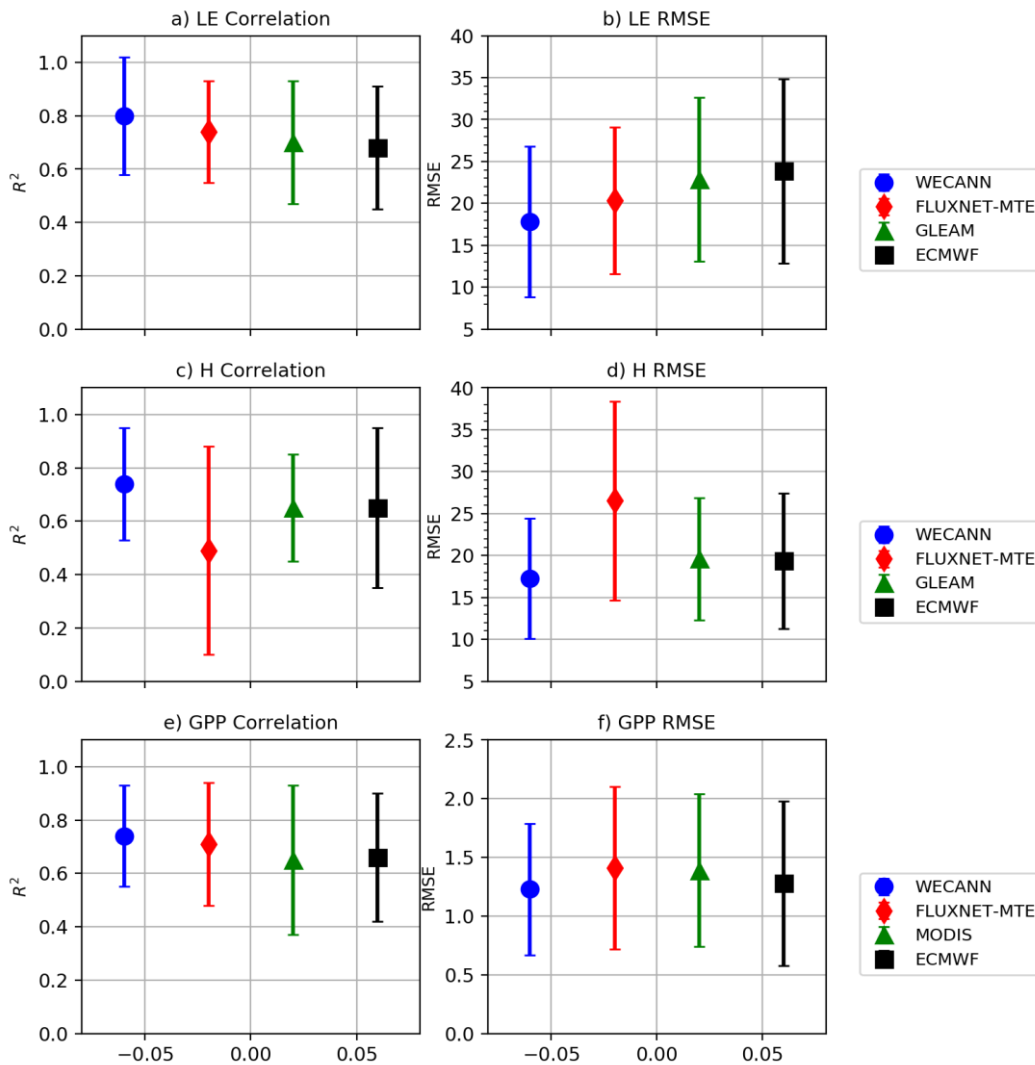
707 3.3. Agricultural Monitoring

708 Two agricultural cases illustrate how TD error can impact both categorical and quantitative
709 remotely sensed measures. The first relates to cropland mapping and is drawn from an ongoing study
710 focused on mapping smallholder agricultural fields at high spatial resolution (3–4 m) in Ghana. The
711 mapping method is based on “active learning”, in which a random forest-based [124,198,199] ML
712 algorithm is iteratively trained and validated by a crowdsourcing platform. This platform enlists
713 human trainers to visually interpret and digitize field boundaries in the imagery (PlanetScope visual
714 and near-infrared surface reflectance [128]) being classified [149,150,198]. During this process, a
715 protocol is used to assess the accuracy of training labels, in which each worker is periodically directed
716 to a training reference site where the field boundaries are already known but are invisible to the
717 worker. Using these training reference sites, the interpreters' maps are then scored using a multi-
718 dimensional accuracy assessment algorithm [150], resulting in an average TD accuracy score for each
719 worker ranging from 0 (complete disagreement with reference) to 1 (perfect agreement). Each label
720 site is mapped by at least five workers, and the resulting worker-specific accuracy scores are used
721 within a Bayesian merging algorithm to combine the five sets of labels into a single consensus label,
722 which is then used to train the random forest classifier. Here we use the worker-specific training
723 accuracy scores to assess the impact of label quality on map accuracy by assessing three variants of
724 two random forest-generated maps, one over Central Ghana (~3400 km²) and one over Northern
725 Ghana (~3100 km²). The first two maps were trained using labels generated by the worker with the
726 least accurate TD, the second two by the most accurate worker, and the third using the consensus
727 labels. The accuracy of each pair of maps was then assessed against the validation set (reserved
728 consensus labels) using the true skill statistic [90] (sensitivity + specificity – 1, with scores ranging
729 from –1 to 1). The results show a substantial difference in accuracy between the maps trained with
730 the least and most accurate workers' labels (Figure 11A), with the former having 7%–9% more skill
731 than the latter, while maps based on consensus labels have ~3% more skill than those of the most
732 accurate workers' labels.

733 The second case relates to remotely sensed crop estimates of wheat yields collected in 48
734 smallholder fields in Bihar, India in 2016–17 [200]. Yield data were collected via eight 2 × 1 m² crop
735 cuts within each field, and PlanetScope-derived green chlorophyll vegetation indices (GCVI) were
736 calculated over each field from imagery collected over four dates during the growing season (13
737 January, 25 February, 12 March, and 14 April 2017). A random forest regression was trained on the
738 yield measured for each field, using the four dates of GCVI values as predictors. To test the effect of
739 TD error on the resulting yield predictions, three types of noise were artificially introduced into the
740 yield data used for training: (1) a systematic 0.5 ton/ha overestimate with randomly distributed errors
741 sampled from a normal distribution with a mean of 0 ton/ha, (2) random noise with standard
742 deviations of 0.5 ton/ha, and (3) random noise with standard deviations of 1 ton/ha. A baseline model
743 fit to unperturbed data was also developed. Each model was trained on three separate randomly
744 selected subsets of 32 perturbed observations, and the predictions were made for the remaining 16
745 held-out (independent) yield observations, which were not perturbed. This three-fold cross
746 validation process was repeated 50 times, with each permutation using a different random seed to
747 construct the folds, in order to achieve stable error metrics. The model performance was assessed by

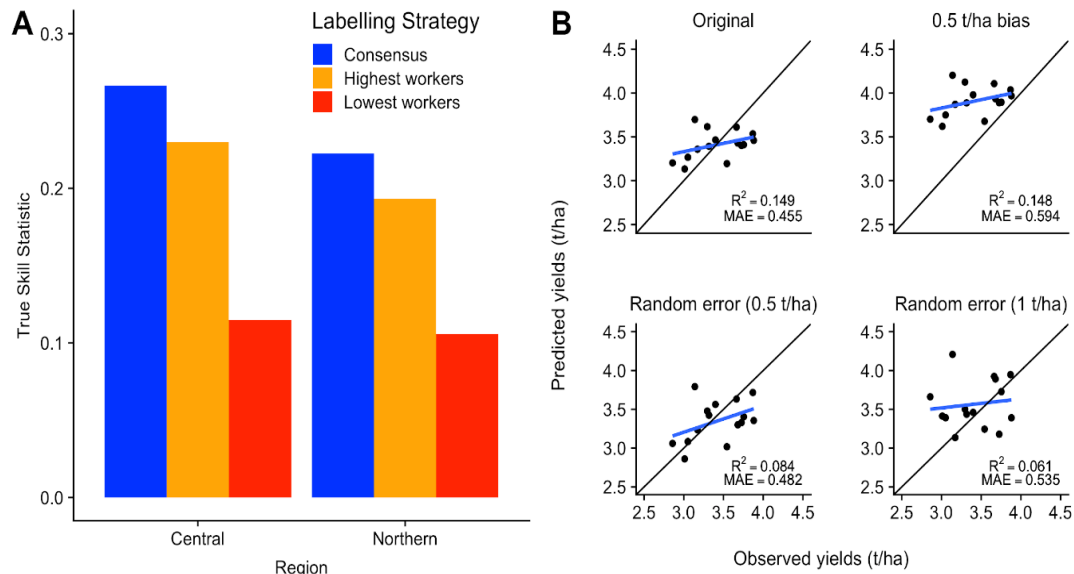
748
749

calculating the averages of the mean absolute error (MAE) of the prediction, and the R^2 of regressions fit between prediction and observed values (Figure 11B).



750
751
752
753
754

Figure 10. Coefficient of determination (R^2) and root mean squared error (RMSE) of the water, energy, and carbon with artificial neural networks (WECANN) model output against ground measurements from FLUXNET towers in comparison to the three datasets used to generate the target training data for latent heat flux (LE) (a, b), sensible heat flux (H) (c, d) and gross primary production (GPP) (e, f).



755

756

757

758

759

760

761

762

763

764

Figure 11. A comparison (A) of the accuracy (based on the true skill statistic) of cropland maps over two areas of Ghana when generated by labels of different levels of quality (red = least accurate workers' labels; orange = most accurate workers' labels; blue = "consensus" labels made by merging all workers' labels). (B) Results from a random forest model of wheat yields trained on satellite-derived vegetation indices, showing the relationship between predicted yield and independent observed yields, in terms of the fit against the line and the regression slope of the relationship (points and regression line represent the mean of a single randomly selected model permutation). The average mean absolute error (MAE) and average regression R^2 s calculated across all permutations are shown for each model.

765

766

767

768

769

770

771

772

The results show that four models, including the baseline, compressed the range of yields, as seen in the shallow slope between observed versus predicted values, but prediction error was 18–31% higher when training yields had either the high level of random or systematic error within them. The smaller amount of random noise only added ~6% error to the predictions, suggesting that RandomForest is tolerant to some training error. Note that the average R^2 of the observed-predicted regression fit was nearly the same for the systematic error case as the baseline, which shows that this metric can be an unreliable measure of performance for quantitative measures, and that it is important to assess fit against the $y = x$ line and to use a metric such as mean absolute error.

773

4. Guidelines and Recommendations

774

775

776

777

778

Our review and case studies show that the impacts of TD error on EO applications can vary, as can the procedures for assessing those impacts. Nevertheless, several best practices and guidelines can be discerned from this work. Below we synthesize a set of suggested steps for minimizing and accounting for TD error, within the context of undertaking and assessing the accuracy of a typical ML-based mapping project.

779

4.1. Step 1: Define Acceptable Level of Accuracy and Choose Appropriate Metric

780

781

782

783

784

785

786

787

As a starting point, researchers should determine the minimum level of accuracy required for their application, using the accuracy metric(s) most appropriate for answering their questions [201]. For example, if the goal of creating a categorical map is to obtain an unbiased area estimate for a particular land cover, it is essential to account for the map's commission and omission errors by adjusting the proportional area estimate of the cover type derived from the map by the proportion of that type estimated from the map reference sample [39,40,57]. For a continuous variable in which the absolute accuracy of the mapped variable is most important, then the mean absolute deviation from the $y = x$ line is more informative than R^2 [93,94].

788 Error in the map reference data should also be factored into the selected accuracy metrics and
789 resulting map-derived measures. Several published methods exist for categorical data (see Section
790 1.2.1). For continuous variables, the fit between the mapped and map reference variables can be
791 assessed using Type 2 regression, which allows for error in the dependent (map reference) variable
792 [202], unlike the more commonly used Type 1 regression. Determining map reference data error is
793 critical to determining overall map accuracy. The error in these data effectively determines the upper
794 limit of achievable map accuracy, as it is difficult (but not impossible; see [47]) to know whether a
795 model's predictions are more accurate than its map reference data; thus if the map reference data are
796 only 90% accurate, then the map can be at most 90% accurate. Acceptable accuracy should thus be
797 determined relative to the accuracy of the map reference data, rather than the implicit assumption of
798 100%, which is widely used since map reference data are usually considered perfect [38,39,47,57,67].

799 Although the above steps relate primarily to concerns about map accuracy assessment, they are
800 essential to establishing best practices for map TD. This is firstly due to the fact that, without
801 undertaking rigorous accuracy assessment as described above, it is not possible to assess fully how
802 TD error impacts map accuracy. And secondly, the processes of map reference data and TD
803 generation are often tightly intertwined and impacted by many of the same sources of error (see
804 Sections 1.2.1–2). The procedures for minimizing and measuring errors in both datasets are thus often
805 the same. Our subsequent recommendations, therefore, cover both training and map reference
806 datasets, except where we indicate necessary distinctions.

807 4.2. Step 2: Minimize Design-Related Errors

808 The next logical step in a mapping project that relies on TD is to design strategies for
809 independently collecting the training and map reference samples. Although there are numerous
810 factors to consider, there are several general aspects of design that can help minimize potential TD
811 errors.

812 4.2.1. Sample Design

813 The first consideration relates to the sampling design itself, meaning where, when, how many,
814 and what type of samples are placed (e.g., simple random, clustered, stratified, systematic,
815 purposive/directed). With respect to the TD, this depends to a certain extent on the requirements of
816 the selected ML algorithm, since various ML algorithms have differing requirements with respect to
817 geographic distribution [53] and class balance of samples, e.g., [e.g. 31,48,80]. Geographic
818 representativeness and the degree to which the TD capture the variability in the feature of interest
819 are also important TD sample design considerations [53,61,150,203]. Continuous TD, particularly
820 those collected in situ, are often point samples. Therefore a sampling protocol should be used to
821 match field measurements and pixel dimensions in order to avoid scaling problems associated with
822 the modifiable areal unit problem [142,143].

823 The road mapping case study above shows the type of errors that can result when maps are
824 trained with samples that do not adequately represent the features in a particular region. TD can in
825 practice be highly localized or relevant for a limited spatial extent or temporal period [160,194]. This
826 problem may continue to become more relevant, given the increase in stock or benchmark training
827 libraries and subsequent attempts to transfer pre-trained models to different regions, time periods,
828 or scales of observation [73,204]. While such benchmark libraries can be of immense benefit as TD for
829 large area EO research, the representativeness of the features of interest should be assessed and
830 augmented as needed, as shown above in the Khartoum model case study (Figure 9D). For some
831 widely-used ML algorithms, such as random forests, the best practice appears to be to train with data
832 collected within the mapping region (e.g., within a particular agroecoregion [55,205]), and to avoid
833 over-generalizing or transferring models to other regions [206]. However, until more published
834 studies are available, it is not clear whether this rule applies to deep-learning models. When using
835 citizen science or crowdsourcing approaches to generate these data, representativeness can be
836 ensured by directing labelers to the selected TD sites, e.g., [e.g. 150], rather than having the
837 interpreters select the regions to map.

838 Samples should also be temporally representative of the imagery that is being classified [61].
839 That is, relative to the imagery being classified, the TD (and map reference) sample should be
840 collected within a window of time that matches the characteristic rate of change of the feature being
841 mapped. This interval can be estimated by measuring the temporal autocorrelation in the feature of
842 interest [207]. For rapidly changing phenomena, such as deforestation events, snow/ice melt, and
843 vegetation coverage during phenological transition, the sample may need to be captured within a
844 few days or weeks of the acquisition of the imagery being classified, whereas for slower-moving
845 features a sample collected within a few years may be sufficient.

846 In cases where training and reference samples are generated simultaneously, it is essential that
847 TD sample design does not undermine the standards required for an independent, probabilistic map
848 reference sample, *sensu* [sensu 67]. This is particularly relevant for extremely large, geographically
849 broad benchmark datasets, which may be used for either TD or map reference data, assuming the
850 specific data set used conforms to the appropriate criteria. Stehman et al. [176] describe procedures
851 for rigorous incorporation of crowdsourced data while maintaining an appropriate probability-based
852 sampling approach specifically for map reference data, and Stehman and Foody [57] explore issues
853 relating to independence between TD and map reference data during sample design. Beyond those
854 considerations, it is important to note that the map reference sample's independence is compromised
855 when it is used to iteratively refine the mapping algorithm. This problem can best be understood
856 within the context of cross validation, which is appropriate for ML parameter tuning, e.g., [e.g. 31].
857 However, when the number of folds exceed one (as in our yield estimation case study; Figure 11B)
858 then the portions excluded from training lose statistical independence and can no longer serve as the
859 map reference [77]. Map reference data independence may also be undermined when training sites
860 are selected iteratively, in order to increase their representativeness and improve ML performance
861 e.g., [55, e.g. 149]. If the gain due to new training sites is assessed against the map reference, then it
862 will also lose independence after the first iteration. Moreover, any error in the map reference sample
863 will be integrated into the final map. Xiong et al. [55] avoided this problem by visually assessing
864 whether their classifier improved map quality after having new TD points added to the initial sample.
865 A more quantitative approach is to divide an initial sample into three splits: one for training, the
866 second for validating algorithm improvements, including those related to the addition of new
867 training sites, and the third as the map reference, used only for final accuracy assessment. This
868 partitioning approach can be implemented in the mapping platform used in the cropland mapping
869 case study, Figure 11A [199].

870 4.2.2. Training Data Sources

871 The requirements for temporal representativeness make the source of training imagery a critical
872 consideration for projects that rely on image interpretation. The use of basemap imagery is not
873 recommended for training maps of dynamic features, given their broad range and uneven
874 distribution of image acquisition dates [61], unless the age of the imagery being classified can be
875 matched to that of the training imagery. Otherwise, there is substantial potential for introducing error
876 into the mapping algorithm (e.g., Figure 1), and its impact may be hard to assess, particularly if the
877 map reference sample is collected from the basemap. The goal of temporal representativeness must
878 be balanced with the need to have a sufficiently high spatial resolution to accurately interpret the
879 smallest target features/classes (i.e., the MMU; see Step 3). Beyond matters of cost, this tradeoff is one
880 reason that HR/VHR basemaps are widely used [61]. Newly available commercial imagery such as
881 PlanetScope [128] are collected at high temporal frequency (near-daily) and have a spatial resolution
882 sufficient for many visual interpretation tasks (3–4 m) and, therefore, may be a preferable source of
883 training imagery for developing maps representing the post-2016 period. Finally, in designing an
884 image-based sample, it is also important to consider additional characteristics that can influence
885 interpreters' judgement, such as atmospheric quality (e.g., clouds, haze), sensor view angle, sun
886 angle, spectral band selection, and image contrast stretches [74].

887 4.2.3. Legend Design

888 For thematic maps, legend design merits special consideration as it relates to TD, particularly
889 for multi-temporal and/or large area projects that rely on multiple image datasets [61]. As discussed
890 in section 2 above, objects of interest, including land-cover patches (i.e., the MMU), should be at least
891 twice as large as the pixel resolution of the imagery used in the classification algorithm, assuming a
892 requirement for spectrally pure pixels [136,168,208]. When image spatial resolution is too coarse
893 relative to the scene elements of interest, image interpretation errors are likely due to mixed pixels
894 [127,137,138]. This implies that in designing a legend, researchers should select classes with an MMU
895 that is large enough to be effectively captured by the coarsest resolution imagery to be incorporated
896 in the model, which will help avoid the problem of collecting training samples with mixed pixels [e.g.
897 55]. This consideration is particularly relevant since HR/VHR imagery is often used to create TD and
898 map reference data, while the mapping algorithm is applied to moderate- or coarse-resolution
899 imagery, e.g., [e.g. 55,120,209,210]. Alternatively, researchers may opt to select a classification
900 workflow which explicitly incorporates mixed pixels, e.g., [98,165,e.g. 173].

901 Spatial representativeness should be considered as a limiting factor for legend design [53], and
902 to the extent possible, researchers should attempt to use categories that are supported by both the
903 spatial resolution of the model data and the field sampling protocols to be used; we recommend that
904 researchers consult the extensive literature on legend design [25,144–147,211–213].

905 4.3. Step 3: Minimize Collection-Related Errors

906 There are numerous ways to collect TD for categorical and continuous mapping projects, each
907 with their own sources of error. There are thus many potential approaches for minimizing the
908 associated collection errors, which may be quite specific to a particular variable (e.g., for agricultural
909 area estimates [214]). However, there are several general approaches that can be followed to minimize
910 TD collection errors. Our focus here is primarily on error in image-interpreted TD, which is one of
911 the most common approaches used to training ML mapping algorithms. We also touch on the specific
912 case of model-derived training data.

913 Whenever possible, we recommend using protocols that incorporate training reference data to
914 independently assess TD accuracy, particularly for image-interpreted TD, e.g., [e.g. 150]. Training
915 reference datasets can be limited in size compared to the ultimate sample size, provided that training
916 reference locations are randomly presented to interpreters during the data creation campaign
917 [150]. Active feedback during training label creation can also help reduce errors on a rolling basis by
918 providing interpreters with information regarding their performance [174].

919 If comparison against training reference data is not possible, then consensus methods for
920 generating TD may be the next best alternative. Consensus between at least 3 interpreters is
921 recommended to allow for majority voting [34,46], but more complex land covers may require up to
922 7 interpreters [46]. Consensus among several domain experts may also be the best and most practical
923 measure for collecting both training reference data and map reference data [34,57]. In the case of
924 image-interpreted samples, consensus approaches should employ multiple interpreters to label the
925 same site. For continuous variables, several independent or repeated in situ measurements should be
926 made and aggregated. For modeled variables where the error is unknown, as in the surface flux case
927 study, training based on the outputs of multiple independent models is recommended. The
928 agricultural case study shows how multiple mappings can be used to quantify label uncertainty
929 (Figure 12A) and minimize the amount of labeling error, yielding improved map accuracy (Figure
930 11A). The surface flux case study demonstrates these same benefits across several continuous
931 variables (Figure 10). The number of separate measures or interpreters needed will vary depending
932 on the application. For example, in the cropland mapping case study, 5 interpreters labeled each
933 consensus training sample, and in the continuous surface flux example, 3 separate modeled inputs
934 were used.

935 Further steps can be taken to minimize TD collection errors arising from image interpretation.
936 Interpreters should be given thorough training regarding the task [34], which may include instruction
937 on remote-sensing principles as well as local or regional contextual information. Local domain
938 expertise is particularly helpful for consistent identification of idiosyncratic land covers [163].

939 Interpreter education is particularly important for crowdsourcing or citizen science data collection
940 campaigns, as participants typically lack formal experience in image interpretation [151,215].

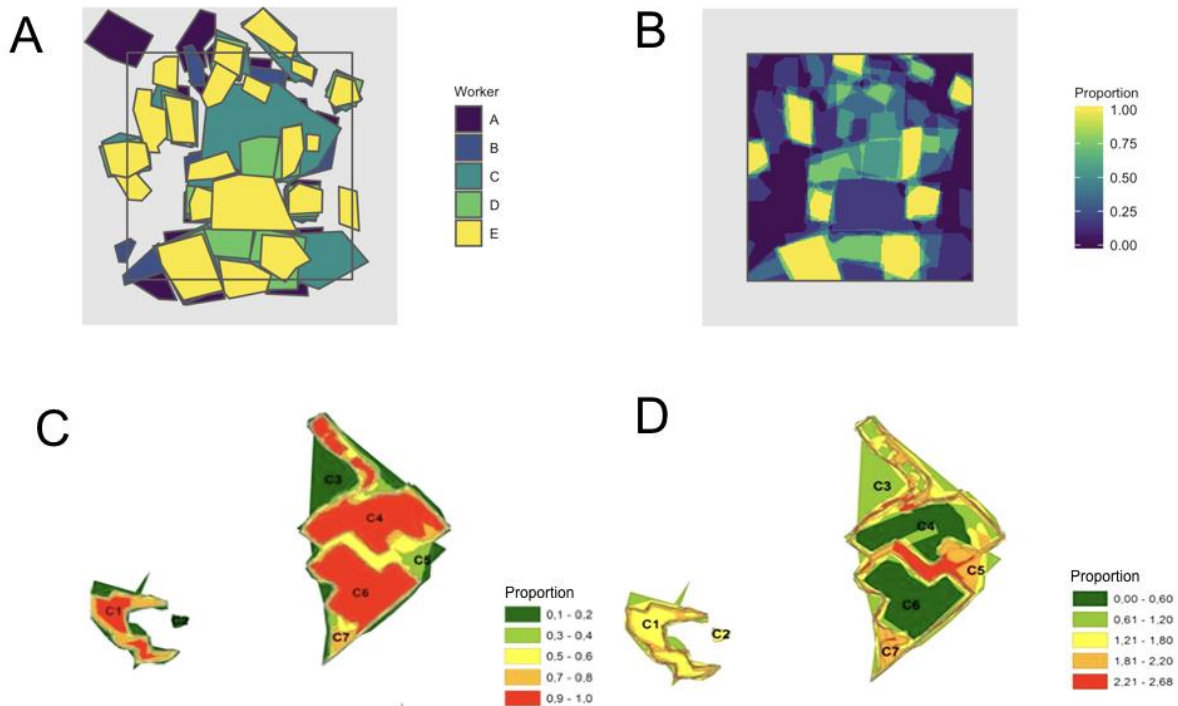
941 As described in Step 2 above, image interpretation is inadvisable when the available imagery
942 does not support the legend categories in terms of spatial, spectral, temporal, or radiometric
943 resolution [216–218]. Researchers must be especially cautious in the similar but potentially more
944 hazardous case that HR/VHR imagery is used to create training samples that are then used with
945 coarser resolution imagery when ingested into the ML model. Assuming that researchers correctly
946 specify their data selection and legend design when using higher spatial resolution imagery to create
947 TD, image interpretation errors due to insufficient resolution should be minimized; however, special
948 care should be given to borderline classes, or classes exhibiting a high degree of spatial and/or
949 spectral variability due to land-cover mixtures within the pixel [127,137,138,154,219]. In such cases,
950 we recommend that training polygons be created near the center of scene objects, where pixel mixing
951 is likely to be minimized, e.g., [e.g. 55].

952 Another important error-minimizing approach relates to cases in which TD comes from a
953 process model, as in the surface flux example outlined above. Process models are also increasingly
954 used to train crop yield mapping models, due to the difficulty of obtaining sufficiently large and
955 reliable field-scale yield data for training [220]. To circumvent this challenge, the scalable yield
956 mapping (SCYM) method [221,222] uses a mechanistic crop model to simulate yields under various
957 environmental and management conditions. The model's outputs then become inputs for training an
958 empirical mapping model (typically ML), in which the simulated yield is the dependent variable and
959 a subset of remotely retrievable model variables serve as predictors. TD errors in such cases can be
960 minimized by rigorously calibrating the process model (itself a challenging task) using best practices
961 from the relevant modeling literature, e.g., [e.g. 223]. Alternatively, if modeled TD are necessary but
962 careful calibration is not possible (e.g., because the data are pre-existing), then a merging approach
963 such as triple collocation (Section 4.2) can help reduce training error.

964 4.4. Step 4. Assess Error in Training Data Error

965 The best way to assess both TD (and map reference data) error is to measure it directly. For
966 continuous variables, calculating measurement error should be possible in many cases, even for
967 model-generated data, in which the variance can be calculated from simulation treatments, e.g., [e.g.
968 223]. For categorical mapping, label error can be measured using an internal accuracy assessment
969 protocol that makes use of predefined training reference data (e.g., Estes et al., [150]).

970 However, it can be challenging to produce training reference data, and indeed in some cases the
971 true category is not clear, whether looking at an image or standing on site. In these cases, or when a
972 direct TD error measurement protocol is not available, we recommend that researchers calculate
973 uncertainty estimates based on repeated measures or multiple interpreter approaches (e.g., the crowd
974 standard deviation [151]) described in Step 3 above (and see Figure 12); this is useful for both training
975 and map reference data. We also recommend that additional measures relating to data collection
976 speed, precision, and consistency be collected for individual data creators, as these can generate
977 further insight into relative TD errors. This recommendation is based on experience in crowdsourced
978 data creation [150,151], but it is applicable to any type of data collection, and could greatly bolster the
979 understanding and quantification of error propagation. If it is not possible to either directly quantify
980 TD error or relative uncertainty, then researchers should at a minimum clearly document the data
981 creation methods, and detail likely sources of error and potential uncertainties.



982

983

984

985

986

987

988

989

990

991

992

Figure 12. Two examples of consensus-based mapping approaches and their potential use for assessing training (or reference) data uncertainty. Panel A shows a collection of crop field boundary polygons drawn by five independent workers around crop fields visible in PlanetScope imagery collected over Ghana. These labels can be converted into a heat map (B) showing the overall agreement, the inverse of uncertainty. Similarly, 19 independent experts were asked to delineate slum settlements in image subset from Cape Town, South Africa. The polygons are converted into overall agreement and the uncertainty is modeled using random sets (C) shows the covering function, which is then used to calculate standard deviation of random set (D). Both these metrics indicate the variability as well as stability in boundaries delineated by different experts. Adapted with permission from Kohli et al. [163].

993

4.5. Step 5. Evaluate and Communicate the Impact of Training Data Error

994

4.5.1. TD Treatment Tiers

995

996

997

998

999

1000

1001

1002

1003

1004

Due to the wide range of remote-sensing research currently underway, a wide variety of TD and classification algorithms are in use. Therefore, it is not possible to specify a single protocol for treatment of TD error. Instead, we outline three tiers that represent different levels of accounting for the impact of TD errors on resulting map products. These three tiers presuppose that researchers follow best practices for map accuracy assessment, which includes selecting the most appropriate, literature-recommended accuracy measure(s), quantifying map reference sample error, and accounting for the impact of map reference data error on the accuracy measures (per Step 1). If these best practices are followed, TD error impacts will already be implicitly accounted for within the accuracy measures, and the selected TD accounting tier will be governed by the purposes of the mapping application.

1005

Tier 1

1006

1007

1008

1009

1010

1011

The optimal TD accuracy assessment, termed Tier 1, involves quantifying TD error using gold standard training reference data (Step 4). This information is then used to quantify various characteristics of the TD sample such as class balance and sample size. It is also used to determine the impacts of collection error stemming from label or measurement errors on model uncertainty and map accuracy (see Sections 1.2.2 and 2.2). For example, the impact of TD error on the certainty of random forest classifications can be assessed using measures derived from the margin function [48].

1012 The impact of TD error on map accuracy should also be assessed by training models with TD adjusted
1013 to reflect the range of measured TD error, as illustrated by our cropland mapping case study, and
1014 with respect to variations in TD sample size and class balance [30,48,149]. This approach can be used
1015 to inform the researcher how much map improvement can be obtained by improving TD quality. As
1016 such, these tests should be performed against the validation sample rather than the map reference
1017 data, in order to preserve the independence of the latter.

1018 We recommend that developers of benchmark TD libraries adhere to the tier 1 guidelines,
1019 keeping in mind that these data sets are likely to be used for a variety of purposes, including as TD
1020 and map reference data. Undertaking such evaluations can provide users important information
1021 about appropriate usage of these data for different ML models and geographies, and whether the
1022 benchmark data are appropriate for use as TD, training reference data, validation data, and/or map
1023 reference data. A rigorous quantification of error in the samples themselves is particularly important,
1024 since such data are often likely to be used as training and/or map reference data. We strongly urge
1025 researchers to consider what purposes these benchmark data sets are appropriate for, and refer the
1026 reader to previously published literature regarding incorporation of non-probabilistic samples [176].
1027 Ideally, this tier should also be followed by the makers of map products intended for widespread
1028 public use, who should also release TD and map reference data that were used during map creation
1029 [57]. This step would allow users full insight into the quality and usability of the map for their own
1030 purposes.

1031 Published TD (and map reference data) should be documented with standard metadata, as
1032 shown in Table S4, including the relevant error metric associated with each observation. The
1033 SpatioTemporal Asset Catalog (STAC, <https://stacspec.org/>) provides a framework for
1034 standardization of metadata for EO data and is increasingly seen as an international standard for
1035 geospatial data.

1036 Tier 2

1037 If it is not possible to directly measure and quantify TD error, the next best approach to account
1038 for TD error is to introduce a plausible range of simulated error into the TD and evaluate its impact
1039 on model uncertainty and map accuracy after training separate models with the perturbed datasets
1040 [e.g. 48]. If multiple workers are tasked with collecting TD for the same site, then the variance in their
1041 data can be calculated [e.g. 151] to derive the uncertainty bounds (e.g., Figure 12). This approach is
1042 demonstrated in the building mapping case study (section 4.1.1), which illustrates the sensitivity of
1043 key accuracy metrics to two different kinds of simulated labeling errors. The wheat yield case study
1044 (see section 4.3) provides an example of this approach for a continuous variable.

1045 This tier may also provide an acceptable standard for both benchmark datasets and publicly
1046 released map products, particularly where absolute error quantification is less important, as well as
1047 for publicly released map products. TD and map reference data should also be made openly available
1048 with standard metadata, as described above, including the uncertainty metric for each observation.
1049 If it is not possible to publish them (e.g., because of privacy concerns), then researchers should
1050 provide documentation that summarizes these data and their uncertainty.

1051 Tier 3

1052 If the TD error quantification in Tiers 1 or 2 are not possible, then researchers should at minimum
1053 publish their TD and map reference data, e.g., [e.g., 55] with accompanying metadata that includes
1054 descriptions of potential errors and uncertainties. If data cannot be made openly available, then
1055 researchers should publish full descriptions of the potential error in the data. Adherence to this tier,
1056 at least the reporting component, should be the minimal standard practice in peer-reviewed, map-
1057 based scientific research.

1058 4.5.2. Communicating Error

1059 Finally, uncertainty in ML-generated maps associated with both TD and map reference error
1060 should be faithfully reported within the maps and accompanying documents. Incomplete error
1061 reporting serves to limit the scientific validity and usefulness of these products [57]. Given that ML-
1062 generated maps are increasingly used by the public and policy domains, we advise makers of widely
1063 used maps to communicate these uncertainties and their consequences in a manner that is clear and
1064 understandable for broad audiences, including non-specialists, so that users can understand the map
1065 and its limitations. In general, we recommend including the error on or very close to the actual map,
1066 whether by means of metrics, the error matrix, and/or by using cartographic techniques for
1067 representing uncertainty. Examples of effective cartographic techniques for conveying uncertainty
1068 include selection of appropriate, intuitive, and color-blind friendly color schemes for classes and
1069 symbols, varying color value and saturation and font/line weight to indicate levels of uncertainty,
1070 use of crisp versus blurred boundaries and symbols to indicate the range of uncertainty, or display
1071 of consensus maps or side-by-side juxtaposition in cases of multiple, mutually exclusive predictions
1072 for the same place and time (e.g., representing differently specified models) [42,43]. Maps of
1073 consensus in training labels can provide valuable uncertainty information to users, such as shown in
1074 Figure 12A,B.

1075 4.5.3. Towards an Open Training Data Repository

1076 For the scientific community, the ideal standard of openness and replicability is to provide a
1077 complete description of TD collection practices, appropriate accuracy metrics, and perhaps most
1078 importantly of all, the raw data. We recommend the creation of a centralized, open source database
1079 of all available and relevant TD, using the details collected in the proposed template (Table S4), and
1080 recorded using the STAC framework. This type of open repository, taking inspiration from similar
1081 large-scale databases for computer vision (ImageNet, SIFT10M Dataset [224,225], and remote sensing
1082 (BigEarthNet, DeepSat, UC Merced Land-Use Dataset [73,226,227], should contain full training
1083 metadata, citations to the peer-reviewed literature, as well as links to downloadable versions of TD
1084 collection protocols. Following the philosophy of free and open source software, we strongly
1085 recommend that researchers embrace open source data, which is the only way by which a study can
1086 be truly reproduced.

1087 5. Conclusions

1088 Current practices in EO research are generally inattentive to the need to evaluate and
1089 communicate the impact of TD error on ML-generated maps. This oversight undermines the goals of
1090 scientific reproducibility and may compromise the insights drawn from the resulting maps.
1091 Improving these practices is important due to the increasing use of TD-intensive ML algorithms,
1092 which have motivated our review and recommendations.

1093 To resolve terminological differences arising from the influence of non-EO disciplines, and to
1094 help contextualize TD considerations relative to established map accuracy assessment practice, we
1095 distinguish between four types of “truth” data used in ML-based mapping projects (training,
1096 validation, training reference, and map reference data), and define the appropriate role for each
1097 (Section 1.2). We identify causes of error in TD as well as map reference data, distinguishing where
1098 these vary (Section 2.1). We then explore the impacts of TD error (Section 2.2) and provide a set of
1099 case studies to illustrate the consequences of such error across a range of ML-based mapping
1100 applications (Section 3).

1101 We then provide a set of guidelines for minimizing error arising from the design and collection
1102 of TD samples, and present recommendations for measuring and accounting for the impact of these
1103 errors (Section 4). Many of these guidelines and procedures also relate to map reference data
1104 generation, and we ground our recommendations in the existing best practices for map accuracy
1105 assignment (Sections 1.2.1 and 4.1). We conclude by defining three tiers of TD error accounting and
1106 reporting standards, which are designed to accommodate a wide range of ML-based mapping
1107 projects. The highest tiers should be adopted when creating open training libraries and public map
1108 products, both of which are increasingly being developed to meet the growing demand for EO-

1109 derived maps. In this context, there is a pressing need to rigorously evaluate the training
 1110 requirements and relative performance of deep-learning models as they become more widely used
 1111 for EO [36]. While TD is more visible in the context of LCLU and other categorical mapping projects,
 1112 the need for rigorous, well-documented TD is also critically important for continuous variable
 1113 applications in Earth System Sciences (e.g., hydrological research [228]). If adopted within the peer-
 1114 reviewed literature, the standards we propose for TD treatment may improve confidence in scientific
 1115 findings drawn from map-based research, which can otherwise be confounded by poorly quantified
 1116 map errors [33,57].

1117 **Supplementary Materials:** The following are available online at www.mdpi.com/xxx/s1, Figure S1: Sample
 1118 prediction results in Kumasi, Ghana. (a) Input imagery. (b) Predictions from the Las Vegas model. (c) Predictions
 1119 from the Khartoum model. (d) Prediction from the Kumasi model. (e) Predictions from the Khartoum Model
 1120 retrained in Kumasi. Figure S2: Schematic of product selection using the Triple Collocation approach. Table S1:
 1121 List of peer-reviewed publications retrieved using Google Scholar search algorithm results. Table S2: Summary
 1122 of commonly used error metrics. Table S3: Quantitative results of comparing each of the three models trained
 1123 for the road detection case in Kumasi, Ghana to the validation labels. Table S4: Template and procedure for
 1124 documenting training data.

1125 **Author Contributions:** This article synthesizes the ideas of the 20 authors resulting from a workshop focused
 1126 on issues of error in training data for Machine Learning approaches in Earth Observation research.
 1127 Conceptualization, L.E. and A.E.; formal analysis and investigation, L.E., H.A., R.A., J.R.E., L.F., D.K., D.L., A.R.,
 1128 L.S., S.Y., Z.Y.; writing—original draft preparation, A.E., L.E., H.A., L.F., D.K., D.L., R.G.P., A.R., Z.Y.; writing—
 1129 review and editing, A.E., L.E., K.C., H.A., R.A., L.F., M.F., M.J., D.K., J.C.L.B., J.M., J.R.; visualization, H.A., R.A.,
 1130 L.F. D.K., A.R., H.S.; supervision, L.E.; project administration, L.E. and A.E.; funding acquisition, L.E., A. R. All
 1131 authors have read and agreed to the published version of the manuscript.

1132 **Acknowledgments:** This work represents a synthesis of findings from a workshop held at Clark University on
 1133 8–9 January 2019. The workshop and subsequent paper writing and development was supported by a grant from
 1134 Omidyar Network’s Property Rights Initiative, now PlaceFund. Additional support for developing methods and
 1135 data presented here was provided by NASA (80NSSC18K0158), the National Science Foundation (SES-1801251),
 1136 National Institute of Standards and Technology (2017-67003-26615), National Institute of Standards and
 1137 Technology Summer Undergraduate Research Fellowship Program, and New York State Department of
 1138 Environmental Conservation (DEC01-T00640GG-3350000). We thank Victoria Gammino for helpful input and
 1139 advice, and David Allen, Ayo Deas, Lucy Hutyra, Clare Kohler, Barry Logan, Jaret Reblin, Ian Smith for
 1140 assistance with fieldwork and data compilation.

1141 References

- 1142 1. Chen, J.; Chen, J.; Liao, A.; Cao, X.; Chen, L.; Chen, X.; He, C.; Han, G.; Peng, S.; Lu, M.; et al. Global Land
 1143 Cover Mapping at 30 m Resolution: A POK-Based Operational Approach. *ISPRS J. Photogramm. Remote*
 1144 *Sens.* **2015**, *103*, 7–27.
- 1145 2. Friedl, M.A.; Sulla-Menashe, D.; Tan, B.; Schneider, A.; Ramankutty, N.; Sibley, A.; Huang, X. MODIS
 1146 Collection 5 global land cover: Algorithm refinements and characterization of new datasets. *Remote Sens.*
 1147 *Environ.* **2010**, *114*, 168–182.
- 1148 3. Song, X.-P.; Hansen, M.C.; Stehman, S.V.; Potapov, P.V.; Tyukavina, A.; Vermote, E.F.; Townshend, J.R.
 1149 Global land change from 1982 to 2016. *Nature* **2018**, *560*, 639–643.
- 1150 4. Mohanty, B.P.; Cosh, M.H.; Lakshmi, V.; Montzka, C. Soil Moisture Remote Sensing: State-of-the-Science.
 1151 *Vadose Zone J.* **2017**, *16*.
- 1152 5. Daudt, R.C.; Le Saux, B.; Boulch, A.; Gousseau, Y. Guided Anisotropic Diffusion and Iterative Learning for
 1153 Weakly Supervised Change Detection. *arXiv [cs.CV]* 2019.
- 1154 6. Hecht, R.; Meinel, G.; Buchroithner, M. Automatic identification of building types based on topographic
 1155 databases – a comparison of different data sources. *International Journal of Cartography* **2015**, *1*, 18–31.
- 1156 7. Zhang, X.; Jayavelu, S.; Liu, L.; Friedl, M.A.; Henebry, G.M.; Liu, Y.; Schaaf, C.B.; Richardson, A.D.; Gray,
 1157 J. Evaluation of land surface phenology from VIIRS data using time series of PhenoCam imagery. *Agric.*
 1158 *For. Meteorol.* **2018**, *256–257*, 137–149.
- 1159 8. Tan, B.; Morissette, J.T.; Wolfe, R.E.; Gao, F.; Ederer, G.A.; Nightingale, J.; Pedelty, J.A. An Enhanced
 1160 TIMESAT Algorithm for Estimating Vegetation Phenology Metrics From MODIS Data. *IEEE Journal of*
 1161 *Selected Topics in Applied Earth Observations and Remote Sensing* **2011**, *4*, 361–371.

- 1162 9. Zhang, X.; Friedl, M.A.; Schaaf, C.B. Global vegetation phenology from Moderate Resolution Imaging
1163 Spectroradiometer (MODIS): Evaluation of global patterns and comparison with in situ measurements:
1164 GLOBAL PHENOLOGY FROM MODIS. *J. Geophys. Res.* **2006**, *111*, 981.
- 1165 10. Schaaf, C.B.; Gao, F.; Strahler, A.H.; Lucht, W.; Li, X.; Tsang, T.; Strugnell, N.C.; Zhang, X.; Jin, Y.; Muller,
1166 J.-P.; et al. First operational BRDF, albedo nadir reflectance products from MODIS. *Remote Sens. Environ.*
1167 **2002**, *83*, 135–148.
- 1168 11. Liu, Y.; Wang, Z.; Sun, Q.; Erb, A.M.; Li, Z.; Schaaf, C.B.; Zhang, X.; Román, M.O.; Scott, R.L.; Zhang, Q.; et
1169 al. Evaluation of the VIIRS BRDF, Albedo and NBAR products suite and an assessment of continuity with
1170 the long term MODIS record. *Remote Sens. Environ.* **2017**, *201*, 256–274.
- 1171 12. Wang, Z.; Schaaf, C.B.; Sun, Q.; Shuai, Y.; Román, M.O. Capturing rapid land surface dynamics with
1172 Collection V006 MODIS BRDF/NBAR/Albedo (MCD43) products. *Remote Sens. Environ.* **2018**, *207*, 50–64.
- 1173 13. Wan, Z. New refinements and validation of the MODIS Land-Surface Temperature/Emissivity products.
1174 *Remote Sens. Environ.* **2008**, *112*, 59–74.
- 1175 14. Jiménez-Muñoz, J.C.; Sobrino, J.A.; Skoković, D.; Mattar, C.; Cristóbal, J. Land Surface Temperature
1176 Retrieval Methods From Landsat-8 Thermal Infrared Sensor Data. *IEEE Geoscience and Remote Sensing*
1177 *Letters* **2014**, *11*, 1840–1843.
- 1178 15. Jean, N.; Burke, M.; Xie, M.; Davis, W.M.; Lobell, D.B.; Ermon, S. Combining satellite imagery and
1179 machine learning to predict poverty. *Science* **2016**, *353*, 790–794.
- 1180 16. Pekel, J.-F.; Cottam, A.; Gorelick, N.; Belward, A.S. High-resolution mapping of global surface water and
1181 its long-term changes. *Nature* **2016**, *540*, 418–422.
- 1182 17. Hansen, M.C.; Potapov, P.; Tyukavina, A. Comment on “Tropical forests are a net carbon source based on
1183 aboveground measurements of gain and loss.” *Science* **2019**, *363*.
- 1184 18. Gutierrez-Velez, V.H.; Pontius, R.G. Influence of carbon mapping and land change modelling on the
1185 prediction of carbon emissions from deforestation. *Environ. Conserv.* **2012**, *39*, 325–336.
- 1186 19. Deng, J.; Dong, W.; Socher, R.; Li, L.-J.; Li, K.; Fei-Fei, L. Imagenet: A large-scale hierarchical image
1187 database. In Proceedings of the 2009 IEEE conference on computer vision and pattern recognition; Ieee,
1188 2009; pp. 248–255.
- 1189 20. Helber, P.; Bischke, B.; Dengel, A.; Borth, D. EuroSAT: A Novel Dataset and Deep Learning Benchmark for
1190 Land Use and Land Cover Classification. *IEEE Journal of Selected Topics in Applied Earth Observations and*
1191 *Remote Sensing* **2019**, 1–10.
- 1192 21. Liu, Q.; Hang, R.; Song, H.; Li, Z. Learning Multiscale Deep Features for High-Resolution Satellite Image
1193 Scene Classification. *IEEE Trans. Geosci. Remote Sens.* **2018**, *56*, 117–126.
- 1194 22. Laso Bayas, J.C.; Lesiv, M.; Waldner, F.; Schucknecht, A.; Duerauer, M.; See, L.; Fritz, S.; Fraisl, D.;
1195 Moorthy, I.; McCallum, I.; et al. A global reference database of crowdsourced cropland data collected
1196 using the Geo-Wiki platform. *Sci Data* **2017**, *4*, 170136.
- 1197 23. Lary, D.J.; Zewdie, G.K.; Liu, X.; Wu, D.; Levetin, E.; Allee, R.J.; Malakar, N.; Walker, A.; Mussa, H.;
1198 Mannino, A.; et al. Machine Learning Applications for Earth Observation. In *Earth Observation Open*
1199 *Science and Innovation*; Mathieu, P.-P., Aubrecht, C., Eds.; Springer International Publishing: Cham, 2018;
1200 pp. 165–218 ISBN 9783319656335.
- 1201 24. Lary, D.J.; Alavi, A.H.; Gandomi, A.H.; Walker, A.L. Machine learning in geosciences and remote sensing.
1202 *Geoscience Frontiers* **2016**, *7*, 3–10.
- 1203 25. Loveland, T.R.; Reed, B.C.; Brown, J.F.; Ohlen, D.O.; Zhu, Z.; Yang, L.; Merchant, J.W. Development of a
1204 global land cover characteristics database and IGBP DISCover from 1 km AVHRR data. *Int. J. Remote Sens.*
1205 **2000**, *21*, 1303–1330.
- 1206 26. Sulla-Menashe, D.; Gray, J.M.; Abercrombie, S.P.; Friedl, M.A. Hierarchical mapping of annual global land
1207 cover 2001 to present: The MODIS Collection 6 Land Cover product. *Remote Sens. Environ.* **2019**, *222*, 183–
1208 194.
- 1209 27. Fortier, J.; Rogan, J.; Woodcock, C.E.; Runfola, D.M. Utilizing Temporally Invariant Calibration Sites to
1210 Classify Multiple Dates and Types of Satellite Imagery. *Photogrammetric Engineering & Remote Sensing* **2011**,
1211 *77*, 181–189.
- 1212 28. Foody, G.M.; Mathur, A. Toward intelligent training of supervised image classifications: directing training
1213 data acquisition for SVM classification. *Remote Sens. Environ.* **2004**, *93*, 107–117.
- 1214 29. Graves, S.J.; Asner, G.P.; Martin, R.E.; Anderson, C.B.; Colgan, M.S.; Kalantari, L.; Bohlman, S.A. Tree
1215 Species Abundance Predictions in a Tropical Agricultural Landscape with a Supervised Classification

- 1216 Model and Imbalanced Data. *Remote Sensing* **2016**, *8*, 161.
- 1217 30. Foody, G.; Pal, M.; Rocchini, D.; Garzon-Lopez, C. The sensitivity of mapping methods to reference data
1218 quality: Training supervised image classifications with imperfect reference data. *International Journal of ...*
1219 **2016**.
- 1220 31. Maxwell, A.E.; Warner, T.A.; Fang, F. Implementation of machine-learning classification in remote
1221 sensing: an applied review. *Int. J. Remote Sens.* **2018**, *39*, 2784–2817.
- 1222 32. Huang, C.; Davis, L.S.; Townshend, J.R.G. An assessment of support vector machines for land cover
1223 classification. *Int. J. Remote Sens.* **2002**, *23*, 725–749.
- 1224 33. Estes, L.; Chen, P.; Debats, S.; Evans, T.; Ferreira, S.; Kuemmerle, T.; Ragazzo, G.; Sheffield, J.; Wolf, A.;
1225 Wood, E.; et al. A large-area, spatially continuous assessment of land cover map error and its impact on
1226 downstream analyses. *Glob. Chang. Biol.* **2018**, *24*, 322–337.
- 1227 34. Pengra, B.W.; Stehman, S.V.; Horton, J.A.; Dockter, D.J.; Schroeder, T.A.; Yang, Z.; Cohen, W.B.; Healey,
1228 S.P.; Loveland, T.R. Quality control and assessment of interpreter consistency of annual land cover
1229 reference data in an operational national monitoring program. *Remote Sens. Environ.* **2019**, 111261.
- 1230 35. Zhu, X.X.; Tuia, D.; Mou, L.; Xia, G.; Zhang, L.; Xu, F.; Fraundorfer, F. Deep Learning in Remote Sensing:
1231 A Comprehensive Review and List of Resources. *IEEE Geoscience and Remote Sensing Magazine* **2017**, *5*, 8–
1232 36.
- 1233 36. Ma, L.; Liu, Y.; Zhang, X.; Ye, Y.; Yin, G.; Johnson, B.A. Deep learning in remote sensing applications: A
1234 meta-analysis and review. *ISPRS J. Photogramm. Remote Sens.* **2019**, *152*, 166–177.
- 1235 37. Foody, G.M. Status of land cover classification accuracy assessment. *Remote Sens. Environ.* **2002**, *80*, 185–
1236 201.
- 1237 38. Foody, G.M. Assessing the accuracy of land cover change with imperfect ground reference data. *Remote*
1238 *Sensing of Environment* **2010**, *114*, 2271–2285.
- 1239 39. Olofsson, P.; Foody, G.M.; Herold, M.; Stehman, S.V.; Woodcock, C.E.; Wulder, M.A. Good practices for
1240 estimating area and assessing accuracy of land change. *Remote Sens. Environ.* **2014**, *148*, 42–57.
- 1241 40. Pontius, R.G.; Millones, M. Death to Kappa: birth of quantity disagreement and allocation disagreement
1242 for accuracy assessment. *Int. J. Remote Sens.* **2011**, *32*, 4407–4429.
- 1243 41. Congalton, R.G.; Green, K. *Assessing the accuracy of remotely sensed data: principles and practices*; CRC press,
1244 2008;.
- 1245 42. Monmonier, M. Cartography: uncertainty, interventions, and dynamic display. *Prog. Hum. Geogr.* **2006**, *30*,
1246 373–381.
- 1247 43. MacEachren, A.M. Visualizing Uncertain Information. **1992**, 10–19.
- 1248 44. Goodchild, M.F.; Gopal, S. *The Accuracy Of Spatial Databases*; CRC Press, 1989; ISBN 9780203490235.
- 1249 45. Congalton, R.G. A review of assessing the accuracy of classifications of remotely sensed data. *Remote Sens.*
1250 *Environ.* **1991**, *37*, 35–46.
- 1251 46. McRoberts, R.E.; Stehman, S.V.; Liknes, G.C.; Næsset, E.; Sannier, C.; Walters, B.F. The effects of imperfect
1252 reference data on remote sensing-assisted estimators of land cover class proportions. *ISPRS J. Photogramm.*
1253 *Remote Sens.* **2018**, *142*, 292–300.
- 1254 47. Carlotto, M.J. Effect of errors in ground truth on classification accuracy. *Int. J. Remote Sens.* **2009**, *30*, 4831–
1255 4849.
- 1256 48. Mellor, A.; Boukir, S.; Haywood, A.; Jones, S. Exploring issues of training data imbalance and mislabelling
1257 on random forest performance for large area land cover classification using the ensemble margin. *ISPRS J.*
1258 *Photogramm. Remote Sens.* **2015**, *105*, 155–168.
- 1259 49. Swan, B.; Laverdiere, M.; Yang, H.L. How Good is Good Enough?: Quantifying the Effects of Training Set
1260 Quality. In Proceedings of the Proceedings of the 2Nd ACM SIGSPATIAL International Workshop on AI
1261 for Geographic Knowledge Discovery; ACM: New York, NY, USA, 2018; pp. 47–51.
- 1262 50. Ghimire, B.; Rogan, J.; Galiano, V.R.; Panday, P.; Neeti, N. An Evaluation of Bagging, Boosting, and
1263 Random Forests for Land-Cover Classification in Cape Cod, Massachusetts, USA. *GISci. Remote Sens.* **2012**,
1264 *49*, 623–643.
- 1265 51. Rodriguez-Galiano, V.F.; Ghimire, B.; Rogan, J.; Chica-Olmo, M.; Rigol-Sanchez, J.P. An assessment of the
1266 effectiveness of a random forest classifier for land-cover classification. *ISPRS J. Photogramm. Remote Sens.*
1267 **2012**, *67*, 93–104.
- 1268 52. Bruzzone, L.; Persello, C. A Novel Context-Sensitive Semisupervised SVM Classifier Robust to Mislabeled
1269 Training Samples. *IEEE Trans. Geosci. Remote Sens.* **2009**, *47*, 2142–2154.

- 1270 53. Cracknell, M.J.; Reading, A.M. Geological mapping using remote sensing data: A comparison of five
1271 machine learning algorithms, their response to variations in the spatial distribution of training data and
1272 the use of explicit spatial information. *Comput. Geosci.* **2014**, *63*, 22–33.
- 1273 54. Mellor, A.; Boukir, S. Exploring diversity in ensemble classification: Applications in large area land cover
1274 mapping. *ISPRS J. Photogramm. Remote Sens.* **2017**, *129*, 151–161.
- 1275 55. Xiong, J.; Thenkabail, P.S.; Tilton, J.C.; Gumma, M.K.; Teluguntla, P.; Oliphant, A.; Congalton, R.G.;
1276 Yadav, K.; Gorelick, N. Nominal 30-m Cropland Extent Map of Continental Africa by Integrating Pixel-
1277 Based and Object-Based Algorithms Using Sentinel-2 and Landsat-8 Data on Google Earth Engine. *Remote*
1278 *Sensing* **2017**, *9*, 1065.
- 1279 56. Bey, A.; Jetimane, J.; Lisboa, S.N.; Ribeiro, N.; Siteo, A.; Meyfroidt, P. Mapping smallholder and large-scale
1280 cropland dynamics with a flexible classification system and pixel-based composites in an emerging
1281 frontier of Mozambique. *Remote Sens. Environ.* **2020**, *239*, 111611.
- 1282 57. Stehman, S.V.; Foody, G.M. Key issues in rigorous accuracy assessment of land cover products. *Remote*
1283 *Sens. Environ.* **2019**, *231*, 111199.
- 1284 58. Zhang, C.; Xie, Z. Object-based Vegetation Mapping in the Kissimmee River Watershed Using HyMap
1285 Data and Machine Learning Techniques. *Wetlands* **2013**, *33*, 233–244.
- 1286 59. Rogan, J.; Franklin, J.; Stow, D.; Miller, J.; Woodcock, C.; Roberts, D. Mapping land-cover modifications
1287 over large areas: A comparison of machine learning algorithms. *Remote Sens. Environ.* **2008**, *112*, 2272–2283.
- 1288 60. Copass, C.; Antonova, N.; Kennedy, R. Comparison of Office and Field Techniques for Validating
1289 Landscape Change Classification in Pacific Northwest National Parks. *Remote Sensing* **2018**, *11*, 3.
- 1290 61. Lesiv, M.; See, L.; Laso Bayas, J.C.; Sturm, T.; Schepaschenko, D.; Karner, M.; Moorthy, I.; McCallum, I.;
1291 Fritz, S. Characterizing the Spatial and Temporal Availability of Very High Resolution Satellite Imagery in
1292 Google Earth and Microsoft Bing Maps as a Source of Reference Data. *Land* **2018**, *7*, 118.
- 1293 62. Biradar, C.M.; Thenkabail, P.S.; Noojipady, P.; Li, Y.; Dheeravath, V.; Turrall, H.; Velpuri, M.; Gumma,
1294 M.K.; Gangalakunta, O.R.P.; Cai, X.L.; et al. A global map of rainfed cropland areas (GMRCAs) at the end
1295 of last millennium using remote sensing. *Int. J. Appl. Earth Obs. Geoinf.* **2009**, *11*, 114–129.
- 1296 63. Mallinis, G.; Emmanoloudis, D.; Giannakopoulos, V.; Maris, F.; Koutsias, N. Mapping and interpreting
1297 historical land cover/land use changes in a Natura 2000 site using earth observational data: The case of
1298 Nestos delta, Greece. *Appl. Geogr.* **2011**, *31*, 312–320.
- 1299 64. Jawak, S.D.; Luis, A.J. Improved land cover mapping using high resolution multiangle 8-band
1300 WorldView-2 satellite remote sensing data. *JARS* **2013**, *7*, 073573.
- 1301 65. Ye, S.; Pontius, R.G.; Rakshit, R. A review of accuracy assessment for object-based image analysis: From
1302 per-pixel to per-polygon approaches. *ISPRS J. Photogramm. Remote Sens.* **2018**, *141*, 137–147.
- 1303 66. Fritz, S.; See, L.; Perger, C.; McCallum, I.; Schill, C.; Schepaschenko, D.; Duerauer, M.; Karner, M.; Dresel,
1304 C.; Laso-Bayas, J.-C.; et al. A global dataset of crowdsourced land cover and land use reference data. *Sci*
1305 *Data* **2017**, *4*, 170075.
- 1306 67. Stehman, S.V. Sampling designs for accuracy assessment of land cover. *Int. J. Remote Sens.* **2009**, *30*, 5243–
1307 5272.
- 1308 68. Brodrick, P.G.; Davies, A.B.; Asner, G.P. Uncovering Ecological Patterns with Convolutional Neural
1309 Networks. *Trends Ecol. Evol.* **2019**, *34*, 734–745.
- 1310 69. Xiao, T.; Xia, T.; Yang, Y.; Huang, C.; Wang, X. Learning from massive noisy labeled data for image
1311 classification. In Proceedings of the Proceedings of the IEEE conference on computer vision and pattern
1312 recognition; cv-foundation.org, 2015; pp. 2691–2699.
- 1313 70. Frénay, B.; Verleysen, M. Classification in the presence of label noise: a survey. *IEEE Trans Neural Netw*
1314 *Learn Syst* **2014**, *25*, 845–869.
- 1315 71. Brodley, C.E.; Friedl, M.A. Identifying Mislabeled Training Data. *1* **1999**, *11*, 131–167.
- 1316 72. Van Etten, A.; Lindenbaum, D.; Bacastow, T.M. SpaceNet: A Remote Sensing Dataset and Challenge
1317 Series. *arXiv [cs.CV]* 2018.
- 1318 73. Sumbul, G.; Charfuelan, M.; Demir, B.; Markl, V. BigEarthNet: A Large-Scale Benchmark Archive For
1319 Remote Sensing Image Understanding. *arXiv [cs.CV]* 2019.
- 1320 74. Lesiv, M.; Laso Bayas, J.C.; See, L.; Duerauer, M.; Dahlia, D.; Durando, N.; Hazarika, R.; Kumar Sahariah,
1321 P.; Vakolyuk, M. 'yana; Blyshchyk, V.; et al. Estimating the global distribution of field size using
1322 crowdsourcing. *Glob. Chang. Biol.* **2019**, *25*, 174–186.
- 1323 75. Fritz, S.; McCallum, I.; Schill, C.; Perger, C.; See, L.; Schepaschenko, D.; van der Velde, M.; Kraxner, F.;

- 1324 Obersteiner, M. Geo-Wiki: An Online Platform for Improving Global Land Cover. *Environmental Modelling*
1325 *& Software* **2012**, *31*, 110–123.
- 1326 76. Goodchild, M.F. Citizens as sensors: the world of volunteered geography. *GeoJournal* **2007**, *69*, 211–221.
- 1327 77. Kohavi, R.; Others A study of cross-validation and bootstrap for accuracy estimation and model selection.
1328 In Proceedings of the Ijcai; Montreal, Canada, 1995; Vol. 14, pp. 1137–1145.
- 1329 78. Olofsson, P.; Foody, G.M.; Stehman, S.V.; Woodcock, C.E. Making better use of accuracy data in land
1330 change studies: Estimating accuracy and area and quantifying uncertainty using stratified estimation.
1331 *Remote Sens. Environ.* **2013**, *129*, 122–131.
- 1332 79. Catal, C. Performance evaluation metrics for software fault prediction studies. *Acta Polytechnica Hungarica*
1333 **2012**, *9*, 193–206.
- 1334 80. Jeni, L.A.; Cohn, J.F.; De La Torre, F. Facing Imbalanced Data--Recommendations for the Use of
1335 Performance Metrics. In Proceedings of the 2013 Humaine Association Conference on Affective
1336 Computing and Intelligent Interaction; 2013; pp. 245–251.
- 1337 81. Kuzera, K.; Pontius, R.G. Importance of Matrix Construction for Multiple-Resolution Categorical Map
1338 Comparison. *GISci. Remote Sens.* **2008**, *45*, 249–274.
- 1339 82. Pontius, R.G.; Thontteh, O.; Chen, H. Components of information for multiple resolution comparison
1340 between maps that share a real variable. *Environ. Ecol. Stat.* **2008**, *15*, 111–142.
- 1341 83. Pontius, R.G.; Parmentier, B. Recommendations for using the relative operating characteristic (ROC).
1342 *Landsc. Ecol.* **2014**, *29*, 367–382.
- 1343 84. Pontius, R.G. Component intensities to relate difference by category with difference overall. *Int. J. Appl.*
1344 *Earth Obs. Geoinf.* **2019**, *77*, 94–99.
- 1345 85. Pontius, R.G., Jr.; Connors, J. Range of Categorical Associations for Comparison of Maps with Mixed
1346 Pixels. *Photogrammetric Engineering & Remote Sensing* **2009**, *75*, 963–969.
- 1347 86. Aldwaik, S.Z.; Pontius, R.G., Jr. Intensity analysis to unify measurements of size and stationarity of land
1348 changes by interval, category, and transition. *Landsc. Urban Plan.* **2012**, *106*, 103–114.
- 1349 87. Pontius, R.G.; Gao, Y.; Giner, N.M.; Kohyama, T.; Osaki, M.; Hirose, K. Design and Interpretation of
1350 Intensity Analysis Illustrated by Land Change in Central Kalimantan, Indonesia. *Land* **2013**, *2*, 351–369.
- 1351 88. Foody, G.M. Harshness in image classification accuracy assessment. *Int. J. Remote Sens.* **2008**, *29*, 3137–
1352 3158.
- 1353 89. Cohen, J. A Coefficient of Agreement for Nominal Scales. *Educ. Psychol. Meas.* **1960**, *20*, 37–46.
- 1354 90. Allouche, O.; Tsoar, A.; Kadmon, R. Assessing the Accuracy of Species Distribution Models: Prevalence,
1355 Kappa and the True Skill Statistic (TSS). *J. Appl. Ecol.* **2006**, *43*, 1223–1232.
- 1356 91. Foody, G.M. Explaining the unsuitability of the kappa coefficient in the assessment and comparison of the
1357 accuracy of thematic maps obtained by image classification. *Remote Sens. Environ.* **2020**, *239*, 111630.
- 1358 92. Willmott, C.J.; Matsuura, K. On the use of dimensioned measures of error to evaluate the performance of
1359 spatial interpolators. *Int. J. Geogr. Inf. Sci.* **2006**, *20*, 89–102.
- 1360 93. Willmott, C.J.; Matsuura, K.; Robeson, S.M. Ambiguities inherent in sums-of-squares-based error statistics.
1361 *Atmos. Environ.* **2009**, *43*, 749–752.
- 1362 94. Willmott, C.J.; Matsuura, K. Advantages of the mean absolute error (MAE) over the root mean square
1363 error (RMSE) in assessing average model performance. *Clim. Res.* **2005**, *30*, 79–82.
- 1364 95. Pontius, R.G., Jr; Si, K. The total operating characteristic to measure diagnostic ability for multiple
1365 thresholds. *Int. J. Geogr. Inf. Sci.* **2014**, *28*, 570–583.
- 1366 96. Fielding, A.H.; Bell, J.F. A review of methods for the assessment of prediction errors in conservation
1367 presence/absence models. *Environ. Conserv.* **1997**, *24*, 38–49.
- 1368 97. Blaschke, T. Object based image analysis for remote sensing. *ISPRS J. Photogramm. Remote Sens.* **2010**, *65*, 2–
1369 16.
- 1370 98. Costa, H.; Foody, G.M.; Boyd, D.S. Supervised methods of image segmentation accuracy assessment in
1371 land cover mapping. *Remote Sens. Environ.* **2018**, *205*, 338–351.
- 1372 99. Powell, R.L.; Matzke, N.; de Souza, C.; Clark, M.; Numata, I.; Hess, L.L.; Roberts, D.A. Sources of error in
1373 accuracy assessment of thematic land-cover maps in the Brazilian Amazon. *Remote Sens. Environ.* **2004**, *90*,
1374 221–234.
- 1375 100. Zhong, B.; Ma, P.; Nie, A.; Yang, A.; Yao, Y.; Lü, W.; Zhang, H.; Liu, Q. Land cover mapping using time
1376 series HJ-1/CCD data. *Sci. China Earth Sci.* **2014**, *57*, 1790–1799.
- 1377 101. Pacifici, F.; Chini, M.; Emery, W.J. A neural network approach using multi-scale textural metrics from very

- high-resolution panchromatic imagery for urban land-use classification. *Remote Sens. Environ.* **2009**, *113*, 1276–1292.
- 1378
1379
1380 102. Abbas, I.I.; Muazu, K.M.; Ukoje, J.A. Mapping land use-land cover and change detection in Kafur local
1381 government, Katsina, Nigeria (1995-2008) using remote sensing and GIS. *Research journal of environmental*
1382 *and Earth Sciences* **2010**, *2*, 6–12.
- 1383 103. Sano, E.E.; Rosa, R.; Brito, J.L.S.; Ferreira, L.G. Land cover mapping of the tropical savanna region in
1384 Brazil. *Environ. Monit. Assess.* **2010**, *166*, 113–124.
- 1385 104. Hu, T.; Yang, J.; Li, X.; Gong, P. Mapping Urban Land Use by Using Landsat Images and Open Social
1386 Data. *Remote Sensing* **2016**, *8*, 151.
- 1387 105. Galletti, C.S.; Myint, S.W. Land-Use Mapping in a Mixed Urban-Agricultural Arid Landscape Using
1388 Object-Based Image Analysis: A Case Study from Maricopa, Arizona. *Remote Sensing* **2014**, *6*, 6089–6110.
- 1389 106. Hu, Q.; Wu, W.; Xia, T.; Yu, Q.; Yang, P.; Li, Z.; Song, Q. Exploring the Use of Google Earth Imagery and
1390 Object-Based Methods in Land Use/Cover Mapping. *Remote Sensing* **2013**, *5*, 6026–6042.
- 1391 107. Al-Bakri, J.T.; Ajlouni, M.; Abu-Zanat, M. Incorporating Land Use Mapping and Participation in Jordan:
1392 An Approach to Sustainable Management of Two Mountainous Areas. *Mt. Res. Dev.* **2008**, *28*, 49–57.
- 1393 108. Liu, J.; Kuang, W.; Zhang, Z.; Xu, X.; Qin, Y.; Ning, J.; Zhou, W.; Zhang, S.; Li, R.; Yan, C.; et al.
1394 Spatiotemporal characteristics, patterns, and causes of land-use changes in China since the late 1980s. *J.*
1395 *Geogr. Sci.* **2014**, *24*, 195–210.
- 1396 109. Yadav, P.K.; Kapoor, M.; Sarma, K. Land Use Land Cover Mapping, Change Detection and Conflict
1397 Analysis of Nagzira-Navegaon Corridor, Central India Using Geospatial Technology. *International Journal*
1398 *of Remote Sensing and GIS* **2012**, *1*.
- 1399 110. da Costa Freitas, C.; de Souza Soler, L.; Sant’Anna, S.J.S.; Dutra, L.V.; dos Santos, J.R.; Mura, J.C.; Correia,
1400 A.H. Land Use and Land Cover Mapping in the Brazilian Amazon Using Polarimetric Airborne P-Band
1401 SAR Data. *IEEE Trans. Geosci. Remote Sens.* **2008**, *46*, 2956–2970.
- 1402 111. Dewan, A.M.; Yamaguchi, Y. Land use and land cover change in Greater Dhaka, Bangladesh: Using
1403 remote sensing to promote sustainable urbanization. *Appl. Geogr.* **2009**, *29*, 390–401.
- 1404 112. Castañeda, C.; Ducrot, D. Land cover mapping of wetland areas in an agricultural landscape using SAR
1405 and Landsat imagery. *J. Environ. Manage.* **2009**, *90*, 2270–2277.
- 1406 113. Griffiths, P.; van der Linden, S.; Kuemmerle, T.; Hostert, P. A Pixel-Based Landsat Compositing Algorithm
1407 for Large Area Land Cover Mapping. *IEEE Journal of Selected Topics in Applied Earth Observations and*
1408 *Remote Sensing* **2013**, *6*, 2088–2101.
- 1409 114. Ge, Y. Sub-pixel land-cover mapping with improved fraction images upon multiple-point simulation. *Int.*
1410 *J. Appl. Earth Obs. Geoinf.* **2013**, *22*, 115–126.
- 1411 115. Gong, P.; Wang, J.; Yu, L.; Zhao, Y.; Zhao, Y.; Liang, L.; Niu, Z.; Huang, X.; Fu, H.; Liu, S.; et al. Finer
1412 resolution observation and monitoring of global land cover: first mapping results with Landsat TM and
1413 ETM+ data. *Int. J. Remote Sens.* **2013**, *34*, 2607–2654.
- 1414 116. Ghorbani, A.; Pakravan, M. Land use mapping using visual vs. digital image interpretation of TM and
1415 Google earth derived imagery in Shrivani-Darasi watershed (Northwest of Iran). *European Journal of*
1416 *Experimental Biology* **2013**, *3*, 576–582.
- 1417 117. Deng, J.S.; Wang, K.; Hong, Y.; Qi, J.G. Spatio-temporal dynamics and evolution of land use change and
1418 landscape pattern in response to rapid urbanization. *Landsc. Urban Plan.* **2009**, *92*, 187–198.
- 1419 118. Otukey, J.R.; Blaschke, T. Land cover change assessment using decision trees, support vector machines and
1420 maximum likelihood classification algorithms. *Int. J. Appl. Earth Obs. Geoinf.* **2010**, *12*, S27–S31.
- 1421 119. Malinverni, E.S.; Tassetti, A.N.; Mancini, A.; Zingaretti, P.; Frontoni, E.; Bernardini, A. Hybrid object-
1422 based approach for land use/land cover mapping using high spatial resolution imagery. *Int. J. Geogr. Inf.*
1423 *Sci.* **2011**, *25*, 1025–1043.
- 1424 120. Rozenstein, O.; Karnieli, A. Comparison of methods for land-use classification incorporating remote
1425 sensing and GIS inputs. *Appl. Geogr.* **2011**, *31*, 533–544.
- 1426 121. Ran, Y.H.; Li, X.; Lu, L.; Li, Z.Y. Large-scale land cover mapping with the integration of multi-source
1427 information based on the Dempster–Shafer theory. *Int. J. Geogr. Inf. Sci.* **2012**, *26*, 169–191.
- 1428 122. Clark, M.L.; Aide, T.M.; Grau, H.R.; Riner, G. A scalable approach to mapping annual land cover at 250 m
1429 using MODIS time series data: A case study in the Dry Chaco ecoregion of South America. *Remote Sens.*
1430 *Environ.* **2010**, *114*, 2816–2832.
- 1431 123. Berberoglu, S.; Akin, A. Assessing different remote sensing techniques to detect land use/cover changes in

- 1432 the eastern Mediterranean. *Int. J. Appl. Earth Obs. Geoinf.* **2009**, *11*, 46–53.
- 1433 124. Breiman, L. Random Forests. *Mach. Learn.* **2001**, *45*, 5–32.
- 1434 125. Freeman, E.A.; Moisen, G.G.; Frescino, T.S. Evaluating effectiveness of down-sampling for stratified
1435 designs and unbalanced prevalence in Random Forest models of tree species distributions in Nevada. *Ecol.*
1436 *Modell.* **2012**, *233*, 1–10.
- 1437 126. Townshend, J.R.; Masek, J.G.; Huang, C.; Vermote, E.F.; Gao, F.; Channan, S.; Sexton, J.O.; Feng, M.;
1438 Narasimhan, R.; Kim, D.; et al. Global characterization and monitoring of forest cover using Landsat data:
1439 opportunities and challenges. *International Journal of Digital Earth* **2012**, *5*, 373–397.
- 1440 127. Shao, Y.; Lunetta, R.S. Comparison of support vector machine, neural network, and CART algorithms for
1441 the land-cover classification using limited training data points. *ISPRS J. Photogramm. Remote Sens.* **2012**, *70*,
1442 78–87.
- 1443 128. Planet Team Planet Application Program Interface: In Space for Life on Earth. San Francisco, CA 2017.
- 1444 129. Manfreda, S.; McCabe, M.F.; Miller, P.E.; Lucas, R.; Pajuelo Madrigal, V.; Mallinis, G.; Ben Dor, E.;
1445 Helman, D.; Estes, L.; Ciruolo, G.; et al. On the Use of Unmanned Aerial Systems for Environmental
1446 Monitoring. *Remote Sensing* **2018**, *10*, 641.
- 1447 130. Toutin, T. Geometric processing of IKONOS Geo images with DEM. In Proceedings of the Proceedings of
1448 ISPRS Joint Workshop “High Resolution Mapping from Space” 2001; pdfs.semanticscholar.org, 2001; pp.
1449 19–21.
- 1450 131. Reinartz, P.; Müller, R.; Schwind, P.; Suri, S.; Bamler, R. Orthorectification of VHR optical satellite data
1451 exploiting the geometric accuracy of TerraSAR-X data. *ISPRS J. Photogramm. Remote Sens.* **2011**, *66*, 124–
1452 132.
- 1453 132. Aguilar, M.A.; Saldaña, M. del M.; Aguilar, F.J. Assessing geometric accuracy of the orthorectification
1454 process from GeoEye-1 and WorldView-2 panchromatic images. *Int. J. Appl. Earth Obs. Geoinf.* **2013**, *21*,
1455 427–435.
- 1456 133. Chen, J.; Zipf, A. DeepVGI: Deep Learning with Volunteered Geographic Information. In Proceedings of
1457 the Proceedings of the 26th International Conference on World Wide Web Companion; International
1458 World Wide Web Conferences Steering Committee: Republic and Canton of Geneva, Switzerland, 2017;
1459 pp. 771–772.
- 1460 134. Kaiser, P.; Wegner, J.D.; Lucchi, A.; Jaggi, M.; Hofmann, T.; Schindler, K. Learning Aerial Image
1461 Segmentation From Online Maps. *IEEE Trans. Geosci. Remote Sens.* **2017**, *55*, 6054–6068.
- 1462 135. Audebert, N.; Le Saux, B.; Lefevre, S. Joint learning from earth observation and openstreetmap data to get
1463 faster better semantic maps. In Proceedings of the Proceedings of the IEEE Conference on Computer
1464 Vision and Pattern Recognition Workshops; 2017; pp. 67–75.
- 1465 136. Strahler, A.H.; Woodcock, C.E.; Smith, J.A. On the nature of models in remote sensing. *Remote Sens.*
1466 *Environ.* **1986**, *20*, 121–139.
- 1467 137. Foody, G.M. Relating the land-cover composition of mixed pixels to artificial neural network classification
1468 output. *Photogramm. Eng. Remote Sens.* **1996**, *62*, 491–498.
- 1469 138. Moody, A.; Gopal, S.; Strahler, A.H. Artificial neural network response to mixed pixels in coarse-
1470 resolution satellite data. *Remote Sens. Environ.* **1996**, *58*, 329–343.
- 1471 139. De Fries, R.S.; Hansen, M.; Townshend, J.R.G.; Sohlberg, R. Global land cover classifications at 8 km
1472 spatial resolution: The use of training data derived from Landsat imagery in decision tree classifiers. *Int. J.*
1473 *Remote Sens.* **1998**, *19*, 3141–3168.
- 1474 140. Hansen, M.C.; Potapov, P.V.; Moore, R.; Hancher, M.; Turubanova, S.A.; Tyukavina, A.; Thau, D.;
1475 Stehman, S.V.; Goetz, S.J.; Loveland, T.R.; et al. High-resolution global maps of 21st-century forest cover
1476 change. *Science* **2013**, *342*, 850–853.
- 1477 141. Kennedy, R.E.; Yang, Z.; Cohen, W.B. Detecting trends in forest disturbance and recovery using yearly
1478 Landsat time series: 1. LandTrendr — Temporal segmentation algorithms. *Remote Sens. Environ.* **2010**, *114*,
1479 2897–2910.
- 1480 142. Oppenshaw, S.; Taylor, P. A million or so correlation coefficients. *Statistical methods in the spatial sciences.*
1481 *Pion, London* **1979**.
- 1482 143. Jelinski, D.E.; Wu, J. The modifiable areal unit problem and implications for landscape ecology. *Landsc.*
1483 *Ecol.* **1996**, *11*, 129–140.
- 1484 144. Weiss, M.; de Beaufort, L.; Baret, F.; Allard, D.; Bruguier, N.; Marloie, O. Mapping leaf area index
1485 measurements at different scales for the validation of large swath satellite sensors: first results of the

- 1486 VALERI project. In Proceedings of the 8th International symposium in physical measurements and remote
1487 sensing, Aussois (France); w3.avignon.inra.fr, 2001; pp. 125–130.
- 1488 145. Tian, Y.; Woodcock, C.E.; Wang, Y.; Privette, J.L.; Shabanov, N.V.; Zhou, L.; Zhang, Y.; Buermann, W.;
1489 Dong, J.; Veikkanen, B.; et al. Multiscale analysis and validation of the MODIS LAI product: I. Uncertainty
1490 assessment. *Remote Sens. Environ.* **2002**, *83*, 414–430.
- 1491 146. Masuoka, E.; Roy, D.; Wolfe, R.; Morisette, J.; Sinno, S.; Teague, M.; Saleous, N.; Devadiga, S.; Justice, C.O.;
1492 Nickeson, J. MODIS Land Data Products: Generation, Quality Assurance and Validation. In *Land Remote*
1493 *Sensing and Global Environmental Change: NASA's Earth Observing System and the Science of ASTER and*
1494 *MODIS*; Ramachandran, B., Justice, C.O., Abrams, M.J., Eds.; Springer New York: New York, NY, 2011;
1495 pp. 509–531 ISBN 9781441967497.
- 1496 147. Cohen, W.B.; Justice, C.O. Validating MODIS terrestrial ecology products: linking in situ and satellite
1497 measurements. *Remote Sens. Environ.* **1999**, *70*, 1–3.
- 1498 148. Fritz, S.; See, L.; McCallum, I.; You, L.; Bun, A.; Moltchanova, E.; Duerauer, M.; Albrecht, F.; Schill, C.;
1499 Perger, C.; et al. Mapping global cropland and field size. *Glob. Chang. Biol.* **2015**, *21*, 1980–1992.
- 1500 149. Debats, S.R.; Estes, L.D.; Thompson, D.R.; Caylor, K.K. *Integrating active learning and crowdsourcing into*
1501 *large-scale supervised landcover mapping algorithms*; PeerJ Preprints, 2017;.
- 1502 150. Estes, L.D.; McRitchie, D.; Choi, J.; Debats, S.; Evans, T.; Guthe, W.; Luo, D.; Ragazzo, G.; Zempleni, R.;
1503 Caylor, K.K. A Platform for Crowdsourcing the Creation of Representative, Accurate Landcover Maps.
1504 *Environmental Modelling & Software* **2016**, *80*, 41–53.
- 1505 151. Waldner, F.; Schucknecht, A.; Lesiv, M.; Gallego, J.; See, L.; Pérez-Hoyos, A.; d'Andrimont, R.; de Maet, T.;
1506 Bayas, J.C.L.; Fritz, S.; et al. Conflation of expert and crowd reference data to validate global binary
1507 thematic maps. *Remote Sens. Environ.* **2019**, *221*, 235–246.
- 1508 152. Bey, A.; Sánchez-Paus Díaz, A.; Maniatis, D.; Marchi, G.; Mollicone, D.; Ricci, S.; Bastin, J.-F.; Moore, R.;
1509 Federici, S.; Rezende, M.; et al. Collect Earth: Land Use and Land Cover Assessment through Augmented
1510 Visual Interpretation. *Remote Sensing* **2016**, *8*, 807.
- 1511 153. Fritz, S.; Sturn, T.; Karner, M.; Moorthy, I.; See, L.; Laso Bayas, J.C.; Fraisl, D. FotoQuest Go: A Citizen
1512 Science Approach to the Collection of In-Situ Land Cover and Land Use Data for Calibration and
1513 Validation.; pure.iiasa.ac.at, 2019.
- 1514 154. Tuia, D.; Pasolli, E.; Emery, W.J. Using active learning to adapt remote sensing image classifiers. *Remote*
1515 *Sensing of Environment* **2011**, *115*, 2232–2242.
- 1516 155. Van Coillie, F.M.B.; Gardin, S.; Anseel, F.; Duyck, W.; Verbeke, L.P.C.; De Wulf, R.R. Variability of
1517 operator performance in remote-sensing image interpretation: the importance of human and external
1518 factors. *Int. J. Remote Sens.* **2014**, *35*, 754–778.
- 1519 156. Johnson, B.A.; Iizuka, K. Integrating OpenStreetMap crowdsourced data and Landsat time-series imagery
1520 for rapid land use/land cover (LULC) mapping: Case study of the Laguna de Bay area of the Philippines.
1521 *Appl. Geogr.* **2016**, *67*, 140–149.
- 1522 157. Neigh, C.S.R.; Carroll, M.L.; Wooten, M.R.; McCarty, J.L.; Powell, B.F.; Husak, G.J.; Enekel, M.; Hain, C.R.
1523 Smallholder crop area mapped with wall-to-wall WorldView sub-meter panchromatic image texture: A
1524 test case for Tigray, Ethiopia. *Remote Sens. Environ.* **2018**, *212*, 8–20.
- 1525 158. Clark, M.L.; Aide, T.M.; Riner, G. Land change for all municipalities in Latin America and the Caribbean
1526 assessed from 250-m MODIS imagery (2001–2010). *Remote Sens. Environ.* **2012**, *126*, 84–103.
- 1527 159. Comber, A.; Fisher, P.; Wadsworth, R. What is land cover? *Environment and Planning* **2005**, *32*, 199–209.
- 1528 160. Kohli, D.; Sliuzas, R.; Kerle, N.; Stein, A. An ontology of slums for image-based classification. *Comput.*
1529 *Environ. Urban Syst.* **2012**, *36*, 154–163.
- 1530 161. Verburg, P.H.; Neumann, K.; Nol, L. Challenges in using land use and land cover data for global change
1531 studies. *Glob. Chang. Biol.* **2011**, *17*, 974–989.
- 1532 162. Weng, Q. Remote sensing of impervious surfaces in the urban areas: Requirements, methods, and trends.
1533 *Remote Sens. Environ.* **2012**, *117*, 34–49.
- 1534 163. Kohli, D.; Stein, A.; Sliuzas, R. Uncertainty analysis for image interpretations of urban slums. *Comput.*
1535 *Environ. Urban Syst.* **2016**, *60*, 37–49.
- 1536 164. Rocchini, D. While Boolean sets non-gently rip: A theoretical framework on fuzzy sets for mapping
1537 landscape patterns. *Ecol. Complex.* **2010**, *7*, 125–129.
- 1538 165. Woodcock, C.E.; Gopal, S. Fuzzy set theory and thematic maps: accuracy assessment and area estimation.
1539 *Int. J. Geogr. Inf. Sci.* **2000**, *14*, 153–172.

- 1540 166. Rocchini, D.; Foody, G.M.; Nagendra, H.; Ricotta, C.; Anand, M.; He, K.S.; Amici, V.; Kleinschmit, B.;
1541 Förster, M.; Schmidtlein, S.; et al. Uncertainty in ecosystem mapping by remote sensing. *Comput. Geosci.*
1542 **2013**, *50*, 128–135.
- 1543 167. Zhang, J.; Foody, G.M. A fuzzy classification of sub-urban land cover from remotely sensed imagery. *Int. J.*
1544 *Remote Sens.* **1998**, *19*, 2721–2738.
- 1545 168. Woodcock, C.E.; Strahler, A.H. The factor of scale in remote sensing. *Remote Sens. Environ.* **1987**, *21*, 311–
1546 332.
- 1547 169. Cracknell, A.P. Review article Synergy in remote sensing-what's in a pixel? *Int. J. Remote Sens.* **1998**, *19*,
1548 2025–2047.
- 1549 170. Pontius, R.G.; Cheuk, M.L. A generalized cross-tabulation matrix to compare soft-classified maps at
1550 multiple resolutions. *Int. J. Geogr. Inf. Sci.* **2006**, *20*, 1–30.
- 1551 171. Silván-Cárdenas, J.L.; Wang, L. Sub-pixel confusion-uncertainty matrix for assessing soft classifications.
1552 *Remote Sens. Environ.* **2008**, *112*, 1081–1095.
- 1553 172. Foody, G.M. The continuum of classification fuzziness in thematic mapping. *Photogramm. Eng. Remote*
1554 *Sens.* **1999**, *65*, 443–452.
- 1555 173. Foody, G.M. Fully fuzzy supervised classification of land cover from remotely sensed imagery with an
1556 artificial neural network. *Neural Comput. Appl.* **1997**, *5*, 238–247.
- 1557 174. Laso Bayas, J.C.; See, L.; Fritz, S.; Sturn, T.; Perger, C.; Dürauer, M.; Karner, M.; Moorthy, I.;
1558 Schepaschenko, D.; Domian, D.; et al. Crowdsourcing In-Situ Data on Land Cover and Land Use Using
1559 Gamification and Mobile Technology. *Remote Sensing* **2016**, *8*, 905.
- 1560 175. Tewkesbury, A.P.; Comber, A.J.; Tate, N.J.; Lamb, A.; Fisher, P.F. A critical synthesis of remotely sensed
1561 optical image change detection techniques. *Remote Sens. Environ.* **2015**, *160*, 1–14.
- 1562 176. Stehman, S.V.; Fonte, C.C.; Foody, G.M.; See, L. Using volunteered geographic information (VGI) in
1563 design-based statistical inference for area estimation and accuracy assessment of land cover. *Remote Sens.*
1564 *Environ.* **2018**, *212*, 47–59.
- 1565 177. Thompson, I.D.; Maher, S.C.; Rouillard, D.P.; Fryxell, J.M.; Baker, J.A. Accuracy of forest inventory
1566 mapping: Some implications for boreal forest management. *For. Ecol. Manage.* **2007**, *252*, 208–221.
- 1567 178. Bland, M.J.; Altman, D.G. Statistics notes: Measurement error. *BMJ* **1996**, *312*, 1654.
- 1568 179. Martin, D. An Introduction to “The Guide to the Expression of Uncertainty in Measurement.” In
1569 *Evaluation of measurement data -- Guide to the expression of uncertainty in measurement*; JCGM: Geneva,
1570 Switzerland, 2008; pp. 1–10.
- 1571 180. Thanh Noi, P.; Kappas, M. Comparison of Random Forest, k-Nearest Neighbor, and Support Vector
1572 Machine Classifiers for Land Cover Classification Using Sentinel-2 Imagery. *Sensors* **2017**, *18*.
- 1573 181. Song, K. Tackling Uncertainties and Errors in the Satellite Monitoring of Forest Cover Change. **2010**.
- 1574 182. Foody, G.M. The impact of imperfect ground reference data on the accuracy of land cover change
1575 estimation. *Int. J. Remote Sens.* **2009**, *30*, 3275–3281.
- 1576 183. Foody, G.M. Ground reference data error and the mis-estimation of the area of land cover change as a
1577 function of its abundance. *Remote Sens. Lett.* **2013**, *4*, 783–792.
- 1578 184. Homer, C. G., Fry, J. A., Barnes, C. A. National land cover dataset (NLCD). *The National Land Cover*
1579 *Database, U.S. Geological Survey Fact Sheet* 2012. U.S. Geological Survey, Reston, VA, USA.
- 1580 185. Menon, S.; Akbari, H.; Mahanama, S.; Sednev, I.; Levinson, R. Radiative forcing and temperature response
1581 to changes in urban albedos and associated CO₂ offsets. *Environ. Res. Lett.* **2010**, *5*, 014005.
- 1582 186. Hutyrá, L.R.; Yoon, B.; Hepinstall-Cymerman, J.; Alberti, M. Carbon consequences of land cover change
1583 and expansion of urban lands: A case study in the Seattle metropolitan region. *Landsc. Urban Plan.* **2011**,
1584 *103*, 83–93.
- 1585 187. Reinmann, A.B.; Hutyrá, L.R.; Trlica, A.; Olofsson, P. Assessing the global warming potential of human
1586 settlement expansion in a mesic temperate landscape from 2005 to 2050. *Sci. Total Environ.* **2016**, *545–546*,
1587 512–524.
- 1588 188. Hardiman, B.S.; Wang, J.A.; Hutyrá, L.R.; Gately, C.K.; Getson, J.M.; Friedl, M.A. Accounting for urban
1589 biogenic fluxes in regional carbon budgets. *Sci. Total Environ.* **2017**, *592*, 366–372.
- 1590 189. Seto, K.C.; Güneralp, B.; Hutyrá, L.R. Global forecasts of urban expansion to 2030 and direct impacts on
1591 biodiversity and carbon pools. *Proc. Natl. Acad. Sci. U. S. A.* **2012**, *109*, 16083–16088.
- 1592 190. Angel, S.; Parent, J.; Civco, D.L.; Blei, A.; Potere, D. The dimensions of global urban expansion: Estimates
1593 and projections for all countries, 2000–2050. *Prog. Plann.* **2011**, *75*, 53–107.

- 1594 191. Coulston, J.W.; Moisen, G.G.; Wilson, B.T.; Finco, M.V.; Cohen, W.B.; Brewer, C.K. Modeling percent tree
1595 canopy cover: a pilot study. *Photogrammetric Engineering & Remote Sensing* **78** (7): 715–727 **2012**, *78*, 715–
1596 727.
- 1597 192. Reinmann, A.B.; Hutyra, L.R. Edge effects enhance carbon uptake and its vulnerability to climate change
1598 in temperate broadleaf forests. *Proc. Natl. Acad. Sci. U. S. A.* **2017**, *114*, 107–112.
- 1599 193. Rolnick, D.; Veit, A.; Belongie, S.; Shavit, N. Deep Learning is Robust to Massive Label Noise. *arXiv [cs.LG]*
1600 2017.
- 1601 194. Nachmany, Y.; Alemohammad, H. Detecting Roads from Satellite Imagery in the Developing World. In
1602 Proceedings of the Proceedings of the IEEE Conference on Computer Vision and Pattern Recognition
1603 Workshops; openaccess.thecvf.com, 2019; pp. 83–89.
- 1604 195. The SpaceNet Catalog SpaceNet on Amazon Web Services (AWS). “Datasets.” The SpaceNet Catalog. Last
1605 modified April 30, 2018. <https://spacenetchallenge.github.io/datasets/datasetHomePage.html>. (accessed on
1606 15 November 2019.)
- 1607 196. Alemohammad, S.H.; Fang, B.; Konings, A.G.; Aires, F.; Green, J.K.; Kolassa, J.; Miralles, D.; Prigent, C.;
1608 Gentine, P. Water, Energy, and Carbon with Artificial Neural Networks (WECANN): A statistically-based
1609 estimate of global surface turbulent fluxes and gross primary productivity using solar-induced
1610 fluorescence. *Biogeosciences* **2017**, *14*, 4101–4124.
- 1611 197. McColl, K.A.; Vogelzang, J.; Konings, A.G.; Entekhabi, D.; Piles, M.; Stoffelen, A. Extended triple
1612 collocation: Estimating errors and correlation coefficients with respect to an unknown target. *Geophys. Res.*
1613 *Lett.* **2014**, *41*, 6229–6236.
- 1614 198. Debats, S.R.; Luo, D.; Estes, L.D.; Fuchs, T.J.; Caylor, K.K. A Generalized Computer Vision Approach to
1615 Mapping Crop Fields in Heterogeneous Agricultural Landscapes. *Remote Sens. Environ.* **2016**, *179*, 210–221.
- 1616 199. Estes, L.D.; Ye, S.; Song, L.; Avery, R.B.; McRitchie, D.; Eastman, J.R.; Debats S R Caylor Improving maps
1617 of smallholder-dominated croplands through tight integration of human and machine intelligence.;
1618 American Geophysical Union, 2019.
- 1619 200. Jain, M.; Balwinder-Singh; Rao, P.; Srivastava, A.K.; Poonia, S.; Blesh, J.; Azzari, G.; McDonald, A.J.;
1620 Lobell, D.B. The impact of agricultural interventions can be doubled by using satellite data. *Nature*
1621 *Sustainability* **2019**, *2*, 931–934.
- 1622 201. Pontius, R.G. Criteria to Confirm Models that Simulate Deforestation and Carbon Disturbance. *Land* **2018**,
1623 *7*, 105.
- 1624 202. Schennach, S.M. Recent Advances in the Measurement Error Literature. *Annu. Rev. Econom.* **2016**, *8*, 341–
1625 377.
- 1626 203. Waldner, F.; De Aballeyra, D.; Verón, S.R.; Zhang, M.; Wu, B.; Plotnikov, D.; Bartalev, S.; Lavreniuk, M.;
1627 Skakun, S.; Kussul, N.; et al. Towards a set of agrosystem-specific cropland mapping methods to address
1628 the global cropland diversity. *Int. J. Remote Sens.* **2016**, *37*, 3196–3231.
- 1629 204. Castelluccio, M.; Poggi, G.; Sansone, C.; Verdoliva, L. Land Use Classification in Remote Sensing Images
1630 by Convolutional Neural Networks. *arXiv [cs.CV]* 2015.
- 1631 205. Azevedo, T., Sr.; Souza, C.M., Jr.; Shimbo, J.; Alencar, A. MapBiomass initiative: Mapping annual land
1632 cover and land use changes in Brazil from 1985 to 2017.; adsabs.harvard.edu, 2018; Vol. 2018.
- 1633 206. Brown, J.F.; Tollerud, H.J.; Barber, C.P.; Zhou, Q.; Dwyer, J.L.; Vogelmann, J.E.; Loveland, T.R.; Woodcock,
1634 C.E.; Stehman, S.V.; Zhu, Z.; et al. Lessons learned implementing an operational continuous United States
1635 national land change monitoring capability: The Land Change Monitoring, Assessment, and Projection
1636 (LCMAP) approach. *Remote Sens. Environ.* **2019**, 111356.
- 1637 207. Estes, L.; Elsen, P.R.; Treuer, T.; Ahmed, L.; Caylor, K.; Chang, J.; Choi, J.J.; Ellis, E.C. The spatial and
1638 temporal domains of modern ecology. *Nat Ecol Evol* **2018**, *2*, 819–826.
- 1639 208. Jensen, J.R.; Cowen, D.C. Remote sensing of urban/suburban infrastructure and socio-economic attributes.
1640 *Photogramm. Eng. Remote Sens.* **1999**, *65*, 611–622.
- 1641 209. Dorais, A.; Cardille, J. Strategies for Incorporating High-Resolution Google Earth Databases to Guide and
1642 Validate Classifications: Understanding Deforestation in Borneo. *Remote Sensing* **2011**, *3*, 1157–1176.
- 1643 210. Sexton, J.O.; Urban, D.L.; Donohue, M.J.; Song, C. Long-term land cover dynamics by multi-temporal
1644 classification across the Landsat-5 record. *Remote Sens. Environ.* **2013**, *128*, 246–258.
- 1645 211. Reis, M.S.; Escada, M.I.S.; Dutra, L.V.; Sant’Anna, S.J.S.; Vogt, N.D. Towards a Reproducible LULC
1646 Hierarchical Class Legend for Use in the Southwest of Pará State, Brazil: A Comparison with Remote
1647 Sensing Data-Driven Hierarchies. *Land* **2018**, *7*, 65.

- 1648 212. Anderson, J.R. *A Land Use and Land Cover Classification System for Use with Remote Sensor Data*; U.S.
1649 Government Printing Office, 1976;.
- 1650 213. Herold, M.; Woodcock, C.E.; Antonio di Gregorio; Mayaux, P.; Belward, A.S.; Latham, J.; Schullius, C.C.
1651 A joint initiative for harmonization and validation of land cover datasets. *IEEE Trans. Geosci. Remote Sens.*
1652 **2006**, *44*, 1719–1727.
- 1653 214. Carletto, C.; Gourlay, S.; Winters, P. From Guesstimates to GPStimates: Land Area Measurement and
1654 Implications for Agricultural Analysis. *J. Afr. Econ.* **2015**, *24*, 593–628.
- 1655 215. See, L.; Comber, A.; Salk, C.; Fritz, S.; van der Velde, M.; Perger, C.; Schill, C.; McCallum, I.; Kraxner, F.;
1656 Obersteiner, M. Comparing the quality of crowdsourced data contributed by expert and non-experts. *PLoS*
1657 *One* **2013**, *8*, e69958.
- 1658 216. Phinn, S.R. A framework for selecting appropriate remotely sensed data dimensions for environmental
1659 monitoring and management. *Int. J. Remote Sens.* **1998**, *19*, 3457–3463.
- 1660 217. Phinn, S.R.; Menges, C.; Hill, G.J.E.; Stanford, M. Optimizing Remotely Sensed Solutions for Monitoring,
1661 Modeling, and Managing Coastal Environments. *Remote Sens. Environ.* **2000**, *73*, 117–132.
- 1662 218. Lu, D.; Weng, Q. A survey of image classification methods and techniques for improving classification
1663 performance. *International Journal of Remote Sensing* **2007**, *28*, 823–870.
- 1664 219. Cingolani, A.M.; Renison, D.; Zak, M.R.; Cabido, M.R. Mapping vegetation in a heterogeneous mountain
1665 rangeland using landsat data: an alternative method to define and classify land-cover units. *Remote Sens.*
1666 *Environ.* **2004**, *92*, 84–97.
- 1667 220. Burke, M.; Lobell, D.B. Satellite-based assessment of yield variation and its determinants in smallholder
1668 African systems. *Proc. Natl. Acad. Sci. U. S. A.* **2017**.
- 1669 221. Jin, Z.; Azzari, G.; You, C.; Di Tommaso, S.; Aston, S.; Burke, M.; Lobell, D.B. Smallholder maize area and
1670 yield mapping at national scales with Google Earth Engine. *Remote Sens. Environ.* **2019**, *228*, 115–128.
- 1671 222. Lobell, D.B.; Thau, D.; Seifert, C.; Engle, E.; Little, B. A Scalable Satellite-Based Crop Yield Mapper. *Remote*
1672 *Sens. Environ.* **2015**, *164*, 324–333.
- 1673 223. Grassini, P.; van Bussel, L.G.J.; Van Wart, J.; Wolf, J.; Claessens, L.; Yang, H.; Boogaard, H.; de Groot, H.;
1674 van Ittersum, M.K.; Cassman, K.G. How Good Is Good Enough? Data Requirements for Reliable Crop
1675 Yield Simulations and Yield-Gap Analysis. *Field Crops Res.* **2015**, *177*, 49–63.
- 1676 224. Russakovsky, O.; Deng, J.; Su, H.; Krause, J.; Satheesh, S.; Ma, S.; Huang, Z.; Karpathy, A.; Khosla, A.;
1677 Bernstein, M.; et al. ImageNet Large Scale Visual Recognition Challenge. *Int. J. Comput. Vis.* **2015**, *115*, 211–
1678 252.
- 1679 225. Fu, X.; McCane, B.; Mills, S.; Albert, M. NOKMeans: Non-Orthogonal K-means Hashing. In *Computer*
1680 *Vision -- ACCV 2014*; Cremers, D., Reid, I., Saito, H., Yang, M.-H., Eds.; Lecture Notes in Computer Science;
1681 Springer International Publishing: Cham, 2015; Vol. 9003, pp. 162–177 ISBN 9783319168647.
- 1682 226. Basu, S.; Ganguly, S.; Mukhopadhyay, S.; DiBiano, R.; Karki, M.; Nemani, R. DeepSat: A Learning
1683 Framework for Satellite Imagery. In Proceedings of the Proceedings of the 23rd SIGSPATIAL International
1684 Conference on Advances in Geographic Information Systems; ACM: New York, NY, USA, 2015; pp. 37:1–
1685 37:10.
- 1686 227. Yang, Y.; Newsam, S. Bag-of-visual-words and spatial extensions for land-use classification. *Proceedings of*
1687 *the 18th SIGSPATIAL international* **2010**.
- 1688 228. Shen, C. A Transdisciplinary Review of Deep Learning Research and Its Relevance for Water Resources
1689 Scientists. *Water Resour. Res.* **2018**, *54*, 8558–8593.



© 2020 by the authors. Submitted for possible open access publication under the terms and conditions of the Creative Commons Attribution (CC BY) license (<http://creativecommons.org/licenses/by/4.0/>).